UNIVERSITY OF CRETE

MASTER'S THESIS

Fiber-optic chemo-sensors for perfluorinated substances sensing

Author:
Vasileios SARAKATSIANOS

Supervisor:
Dr. Stavros PISSADAKIS

A thesis submitted in fulfillment of the requirements
for the degree of Master of Science
in the Graduate Program of Photonics - Nanoelectronics

September 27, 2022

UNIVERSITY OF CRETE

Abstract

Faculty of Physics

Department of Applied Sciences and Technology

Master of Science

Fiber-optic chemo-sensors for perfluorinated substances sensing

by Vasileios SARAKATSIANOS

From packaging in food industry to medicine and even warfare, per- and polyfluoroalkyl substances find a wide use of applications in our lives. Due to their high chemical and thermal stability, fluorine compounds are commonly used in cooking utensils and the automobile industry as surfactants to waterproof ceramic/metal surfaces.

However, their high stability makes them very resistant to biological degradation, which results in their bioaccumulation in ground water and living organisms. A means to accurately monitor the concentrations of such chemical compounds is necessary to assure general public health and protect the environment.

In this master thesis, a fiber-optic chemo-sensor for perfluorinated substance sensing is presented. A tilted optical fiber Bragg grating was inscribed in a SMF-28 optical fiber and was overlaid with a P(VDF-TrFE-CTFE) polymer film, acting as a transduction layer. The sensor was tested using two different perfluorinated chemicals, trifluorethanol vapors and perfluorooctanoic acid aqueous solutions. Concentrations of said substances, as low as 2 ppm, were able to be detected. A study of the sensor's sensitivity depending on the P(VDF-TrFE-CTFE) polymer film's structural phase (amorphous, crystalline, thermally poled) is also presented. The basic theory regarding its principle of operation and the stages of its development are laid out.

Acknowledgements

I would like to acknowledge and give my warmest thanks to my supervisor, Dr. Stavros Pissadakis, for without his help and guidance this work wouldn't have been possible. His assistance and support was continuous throughout our cooperation, in matters academic and not.

On the same note, I would like to thank Dr. Eleni Pavlopoulou for her time and lending us her expert knowledge regarding the P(VDF–TrFE–CTFE) polymer. Her insight was truly invaluable and much appreciated.

Moreover, I would like to express my sincere gratitude to Dr. Maria Vamvakaki for graciously providing us with the trifluoroethanol needed for our experiments and providing us with her expertise whenever we required it.

Furthermore, I would like to take a moment to thank Dr. Mary Konstantaki for her assistance and guidance in all matters and especially in the grating fabrication process. It goes without saying that without her help this work wouldn't be possible.

Also, I would be remiss if I didn't thank Dimitris Dolapsakis and Nikos Korakas for their valuable assistance with my experiments and their overall support in my endeavors.

Finally, I would like to thank and show my appreciation to my parents, Nikos and Anastasia, for their continuous support and understanding.

Contents

List of Figures

Chapter 1

Introduction

1.1 Optical fiber Bragg grating chemo-sensors

The need for miniaturisation and better precision in sensing systems has made optical fibers a subject of great interest in the field of sensing. Optical fibers offer a versatile, compact, precise and cost-effective sensing platform which can be used in the sensing of numerous physical (eg. strain [1], temperature [2], magnetic field [3]) and chemical (eg. pH [4], salinity [5], humidity [6], concentration of a selected chemical [7]) quantities. The ability to remotely monitor physio-chemical effects, in harsh environments, remotely has garnered great interest for such sensors, for applications in various fields of industry, transportation [8], security and defence [9] [10], medicine [11], environmental monitoring [12] [13] as well as biosensing [14] [15].

In principle, silicate glass optical fibers are resistant to most organic and inorganic chemicals. In order to fabricate a chemo-sensor using an optical fiber one usually needs a transduction material to interact with the chemical species to be detected, and an optical platform/element (Bragg or long-period grating) to detect the changes introduced in the transducer. Picking an ideal transducer is critical to developing a successful chemo-sensor as it can help trace specific chemicals while shielding the fiber from other substances and by making our readout signal more pronounced [16].

As mentioned in the previous paragraph, fiber Bragg gratings (FBG) and particularly, tilted optical fiber Bragg gratings (TOFBG) make for ideal optical platforms for

the development of optical fiber chemo-sensors. A FBG consists of a periodic variation in the refractive index of an optical fiber's core, which produces a wavelength-specific dielectric mirror. FBGs find a wide use of applications in laser technology, telecommunications and sensing [17]. In the case of TOFBGs, a certain tilt is introduced between the grating plane and the fiber cross section. The existence of tilt angle leads to the excitation of modes with azimuthal components resulting in a transmission spectrum with a great number of strong cladding mode notches, which in turn can be used for multi-parameter sensing after their interaction with the out-cladding environment. This fact makes TOFBGs ideal platforms for the development of chemo- and bio- sensors [18] [19].

1.2 Sensor description and motivation

Fluorinated substances are widely used in many aspects of daily life, mainly in specialty paints for achieving hydrophobic performance, in waterproof fabrics and uniforms, also in medical applications as inhaled anesthetics (ie isoflurane).

Despite their many uses, fluoride-rich chemical substances can pose numerous threats to public health and the environment. Perfluorinated chemicals are highly persistent pollutants that tend to accumulate on groundwater and even living organisms. Monitoring their local concentration through collecting and chemically analysing water samples, could provide us with valuable insight on how the contamination is evolving in a certain area. This could prove especially crucial in areas with heavy industry, where large amounts of wastes end up in groundwater. However, collecting contaminated water samples by hand is neither effective nor safe. Testing a water sample for fluorinated substances is usually done either by using special fluoride testing strips or fluoride reactive dyes. The results of these tests are usually read using a colour chart or a photometer [20]. It is obvious that, by using a colour chart one can only get a rough estimate of the fluorinated substance levels in a water sample and not an accurate reading. On another aspect, fluorinated substances are known to be used for military purposes, mostly as precursors for synthesizing nerve gaseous agents/weapons (i.e. Sarin gas) [21]. Though such uses are banned from the international community, there have been instances that fluorine

based substances have been used by terrorist cells to cause harm to civilian population [22]. Therefore, there are several reasons for considering perfluorochemicals as high importance materials in the sectors of safety, security and environmental protection.

The reasons listed above make the development of a reliable sensing device, to monitor in real time the concentration of such substances, a necessity. Optical fiber chemo-sensors could prove a reliable and cost-effective medium to monitor food, water and public areas from a safe distance, in real time.

In this thesis, the development of such sensor is presented. Specifically, a TOFBG chemo-sensor, sensitive to perfluorinated substances. This sensor consists of a TOFBG whose grating area is overlaid with a thin film of poly (vinylidene fluoride-trifluoroethylene-chlorotrifluoroethylene) [P(VDF-TrFE-CTFE)], a co-polymer of poly (vinylidene fluoride) (PVDF). PVDF and its co-polymers display ferroelectric properties either intrinsically or through proper treatment. The surface charge on PVDF can help in binding with perfluorinated substances in aqueous or gaseous solutions through dipole-dipole or hydrophobic interactions. Perfluorinated substances are strongly polar due to the fluoride molecules they contain while some of them, like PFOA, have octyl groups which are strongly hydrophobic [23].

Two different perfluorinated chemicals were used for our experiments: TFE and PFOA. Among its many uses (solvent for peptides and proteins, used for NMR-based protein folding studies,used in the manufacture of nylon [24]), TFE is the key precursor in developing the drug Forane (Isoflurane), which is used for general anesthesia[25]. Monitoring the exact amount of anesthetic that is delivered to a patient could be crucial for their post surgical resuscitation. This is particularly challenging with gas anesthetics, as gas molecules tend to physisorb to electrically charged surfaces, like the breathing tubes used to administer them, affecting their final concentration reaching the alveoli. On the other hand, PFOA is used in industrial applications (used to manufacture chemicals used in non-stick and stain-resistant coatings, fire-fighting foams, and as a surfactant in industrial processes [26]) and is one of the environmental pollutants discussed in the paragraphs above.

To test the sensor, TFE was placed inside a gas chamber along with the sensor and was let to evaporate. The spectral changes of our sensor versus time, were recorded.

To be specific, a gradual shift of the sensor's spectrum towards smaller wavelengths, was observed. Furthermore, aqueous solutions of PFOA were prepared and were used to submerge our sensors in them, in order to observe the spectral changes in this case. The P(VDF-TrFE-CTFE) polymer film, underwent different physical treatments (annealing and thermal poling) in order to test our sensor's response versus the polymer's phase (amorphous, crystalline, thermally poled). For both chemicals, the polymer film-substance attraction is suspected to be strong enough to not only affect our system optically, due to refractive index change, but also mechanically, due to strain introduced by the P(VDF-TrFE-CTFE) polymer film from interacting with the molecules of the perfluorinated substances.

Apart from applications in environmental protection, applications in medicine are also possible. Specifically, in monitoring the amount of a perfluorinated drug a patient is receiving. For example, in the case of Forane, our sensor could be inserted through a breathing tube, while reaching the lower respiration parts of lung (possibly down to the alveoli scale), for precisely monitoring the anesthetic concentration final provided to the patient.

1.3 Thesis outline

The basic theory and propagation equations regarding optical fibers and tilted fiber gratings is provided in Chapter 2. In Chapter 3, the experimental process and apparatus used, is presented. Specifically, the grating fabrication process and the setup used to produce TOFBGs, the various post inscription fabrication processes upon the TOFBGs and the P(VDF-TrFE-CTFE) polymer film, the experimental setups used to test the sensor's functionality and the properties and uses of the various chemicals used, are laid out. In Chapter 4, the experimental results are presented and discussed. Finally, in Chapter 5, we append the conclusions emerging from this research work.

Chapter 2

Basic Theory

2.1 Introduction to optical fibers

An optical fiber is a flexible, transparent fiber made, typically, by drawing silica glass or plastic to a diameter from a few to a few dozen microns, depending on the actual application the fiber is used for. Optical fibers are most often used to transmit light from one end of the fiber to the other. Optical fibers are mostly known for their ability to transmit information over very long distances, without significant loses, at higher bandwidths. These characteristics have made them invaluable tools in the area of telecommunications. Beside telecommunications, specially designed-modified optical fibers are used as fiber optic sensors and are used in the construction of fiber lasers, for imaging applications etc [27].

2.1.1 Standard optical fibers

Optical fibers consist of a core, were the light is transmitted, and a cladding that surrounds the core. The cladding is in turn coated with a protective plastic called "buffer". Buffers are applied during the draw process and play an important role in keeping the functioning part of the optical fiber clean and shielded from the environment. If additional protection is required, the fibers can be encapsulated in a plastic sleeve called "jacket"[28].

The propagation of light inside the core of an optical fiber is based on total internal reflection. The core has a larger refractive index (n_{co}) than the cladding (n_{cl}) where the refractive index change between core and cladding can be abrupt (step-index fiber) or gradual (graded index fiber). When light traveling in an optically

dense medium hits a boundary at a steep angle (larger than the critical angle for the boundary, θ_{crit}), the light is completely reflected (from Snell's law, $\sin\theta_{crit} = n_{cl}/n_{co} \Rightarrow \theta_{crit} = \arcsin(n_{cl}/n_{co})$). This effect is used in optical fibers to confine light in the core. Light travels through the fiber core, bouncing back and forth off the boundary between the core and cladding[29][30].

Because the light must strike the boundary with an angle greater than the critical angle (θ_{crit}), only light that enters the fiber within a certain range of angles can travel down the fiber without escaping the fiber. This range of angles is called the acceptance cone of the fiber. There is a maximum angle from the fiber axis at which light may enter the fiber so that it will propagate, or travel, in the core of the fiber. The size of this acceptance cone is a function of the refractive index difference between the fiber's core and cladding [31]. Fibers that support many propagation paths or transverse modes are called multi-mode fibers (MMF), while those that support a single mode are called single-mode fibers (SMF) [32].

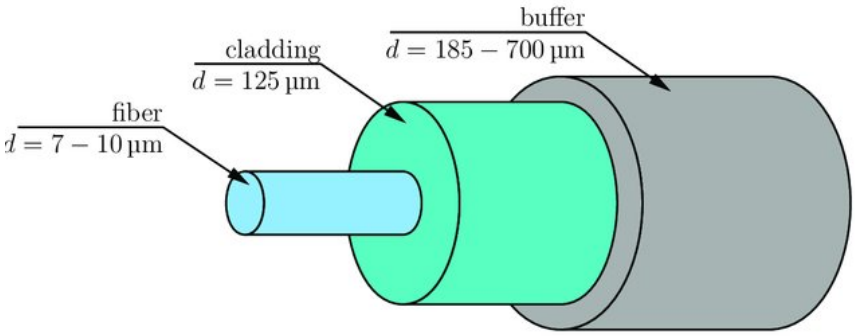

FIGURE 2.1: Structure of a standard SMF [33]

2.1.2 Waveguided modes

By using simple geometric optics one can adequately analyse the propagation of light inside a MMF. The same cannot be done for SMFs though because for media with small V-numbers the geometric optics approach becomes considerably inaccurate [34]. Maxwell's equations must be solved to produce exact solutions for the dielectric cylinder. But such solutions are not easy to produce analytically and are

too complicated to be of any practical use. To amend all these issues a simplified approach to determine the structural characteristics that a fiber must have to produce specific modal properties is needed.

We will assume that the waveguide we study is weakly guiding, meaning that the core and the cladding refractive indices are almost equal ($n_{cl} \approx n_{co}$). Consider a cylindrical core with n_{co}, like the one depicted in Fig.1, with a radius a. Let the cladding be infinite with n_{cl}. The propagation constant β for guided modes can take values between:

$$n_{cl}k \leq \beta \leq n_{co}k \tag{2.1}$$

where $k = 2\pi/\lambda$ is the wavenumber in free space. We also define the core modal parameter u and the cladding modal parameter w:

$$u = a(k^2 n_{co}^2 - \beta^2)^{\frac{1}{2}} \tag{2.2}$$

$$w = a(\beta^2 - k^2 n_{cl}^2)^{\frac{1}{2}} \tag{2.3}$$

The quadratic summation of those two parameters produces a new one called V-number (it can be viewed as some kind of normalized frequency).

$$V = ak(n_{co}^2 - n_{cl}^2)^{1/2} \tag{2.4}$$

We also define the refractive index contrast Δ which, for the case of weak guidance is:

$$\Delta = \frac{n_{co} - n_{cl}}{n_{co}} \ll 1 \tag{2.5}$$

For very small Δ we can formulate modes that are polarized on one direction only.

Without going into much detail we give the longitudinal (z) and transverse (ϕ) field components in cylindrical coordinates.

$$\begin{aligned} E_z = \frac{-iE_l}{2ka}\Bigg\{ & \frac{u}{n_{co}}\frac{J_{l+1}(ur/a)}{J_l(u)}sin(l+1)\phi \\ & + \frac{u}{n_{co}}\frac{J_{l-1}(ur/a)}{J_l(u)}sin(l-1)\phi \\ & + \frac{w}{n_{cl}}\frac{K_{l+1}(wr/a)}{K_l(w)}sin(l+1)\phi \\ & - \frac{w}{n_{cl}}\frac{K_{l-1}(wr/a)}{K_l(w)}sin(l-1)\phi\Bigg\} \end{aligned} \tag{2.6a}$$

$$\begin{aligned} H_z = \frac{-iE_l}{2ka_0}\Bigg\{ & u\frac{J_{l+1}(ur/a)}{K_l(u)}cos(l+1)\phi \\ & - u\frac{J_{l-1}(ur/a)}{J_l(u)}cos(l-1)\phi \\ & + w\frac{K_{l+1}(wr/a)}{K_l(w)}cos(l+1)\phi \\ & - w\frac{K_{l-1}(wr/a)}{K_l(w)}cos(l-1)\phi\Bigg\} \end{aligned} \tag{2.6b}$$

$$E_\phi = \frac{1}{2}E_l \begin{Bmatrix} \frac{J_l(ur/a)}{J_l(u)} \\ \frac{K_l(wr/a)}{K_l(w)} \end{Bmatrix} (cos(l-1)\phi + cos(l+1)\phi) \tag{2.6c}$$

$$H_\phi = -\frac{1}{2}\frac{E_l}{0} \begin{Bmatrix} \frac{n_{co}J_l(ur/a)}{J_l(u)} \\ \frac{n_{co}K_l(wr/a)}{K_l(w)} \end{Bmatrix} (sin(l+1)\phi - sin(l-1)\phi) \tag{2.6d}$$

where $J_l(ur/a)$ are Bessel functions used to describe the modal field inside the core, $K_l(wr/a)$ are Henkel functions used to describe the modal field outside the core, Z_0 is the plane wave impedance in vacuum and E_l is the electrical field strength at the core-cladding interface.

Because Δ is considered to be small the longitudinal components are small compared to the transverse ones. Based on that, we can assume that our modes are linearly polarized (LP).

By setting $n_{co} = n_{cl}$ in equations (2.6) we arrive at the equation:

$$u\frac{J_{l-1}(u)}{J_l(u)} = -w\frac{K_{l-1}(w)}{K_l(w)} \tag{2.7}$$

which is the characteristic equation for the LP modes.

Using that $V^2 = u^2 + w^2$ and differentiating eq. (2.7) with respect to V we get:

$$\partial u/\partial V = (u/V)(1 - \kappa_l) \tag{2.8}$$

where $\kappa_l = K_{l^2}(w)/K_{l-1}(w)K_{l+1}(w)$. By using appropriate approximations we can calculate $u_(V)$ from eq.(2.8) for all modes. For higher order modes we have:

$$u(V) = u_c exp[arcsin(s/u_c) - arcsin(s/V)]/s \tag{2.9}$$

where u_c is the cutoff value of u and $s = (u_c^2 - l^2 - 1)^{1/2}$.

While, for LP_{01}:

$$u(V) = (1 + \sqrt{2})V/[1 + (4 + V^4)^{1/4}] \tag{2.10}$$

Using u(V) we can calculate the values of propagation constant β from eq. (2.2). To make our results universal and not dependant to specific fiber configurations we will not plot β directly but the rati:

$$b(V) = 1 - (u^2/V^2) = [(\beta^2/k^2) - n^2]/(n_{co}^2 - n^2) \tag{2.11}$$

which in the weakly guidance regime becomes:

$$b(V) \approx [\beta/k - n]/(n_{co} - n_{cl}) \tag{2.12}$$

From eqs. (2.5) and (2.12) we obtain β:

$$\beta = nk[1 + \Delta - \Delta(u^2/V^2)] \tag{2.13}$$

By plotting b(V) we can get some interesting information about SMFs.

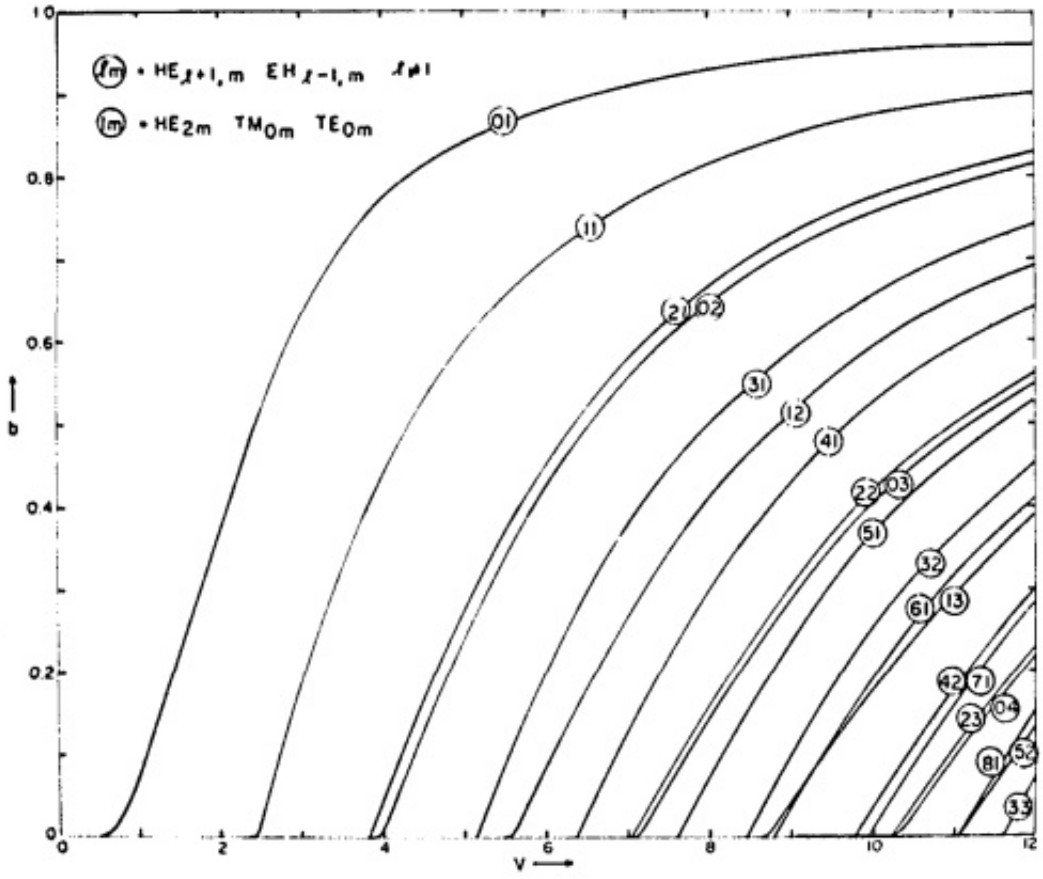

FIGURE 2.2: Normalized propagation parameter b = $(\beta/k - n)/(n_{co} - n_{cl})$ as a function of the normalized frequency V [35].

From that diagram we deduce that there is only a set values V for which only the LP_{01} mode is propagated. These values are between 0 and 2.405. This is a specific limit for the optical fiber engineers which defines the possible values of a, n_{co} and n_{cl} for an optical fiber to be SMF[35]. So, for a specific numerical aperture the core diameter has a very specific range for a fiber to be single mode.

2.2 Fiber Gratings

While the field of fiber optic telecommunications and the use of optical fibers in general has flourished over the years the need to integrate basic optical components like mirrors, filters etc. has remained a challenge for fiber optic science. In most common optical setups (i.e. interferometers, telescopes etc.) light can be focused, dispersed or manipulated in any way we wish using optical components like mirrors, lenses

etc. The same cannot be done for optical fibers where light travels inside a rigid medium.

This has all changed, however, with the discovery of photosensitivity of optical fibers to UV light. By exposing fibers to UV light with characteristic wavelength and intensity the core refractive index of a SMF can be changed to a spatially defined area of the fiber. Due to the difference between the refractive index of the the core and the UV-exposed area light can be reflected in the interface, thus creating a type of dielectric, wavelength-specific, mirror inside the core of the fiber. The wavelengths satisfying the Bragg condition:

$$\frac{2\pi}{\Lambda} = 2\frac{2\pi n_{eff}}{\lambda_B} \Rightarrow \lambda_B = 2n_{eff}\Lambda \tag{2.14}$$

where n_{eff} is the effective refractive index, λ_B is the Bragg wavelength and Λ is the FBG period, will be reflected, while all the other wavelengths will not be affected by the FBG[17]. Fiber gratings are a, usually, periodic spatial modulation of the refractive index of a fiber in a specific area of the fiber core, over a predefined length. Fiber gratings have a significant role to play in telecommunications where they are used as filters to reflect or disperse light. As sensors, fiber gratings have been proven to be especially sensitive to temperature and strain effects as these perturbations lead to changes of the refractive index of the grating planes changing the phase matching conditions leading to wavelength depended reflectivity [36].

2.2.1 Basic theory on fiber gratings

While a plethora of gratings exist depending on the structure of the grating's wave fronts we will focus on two of the most common types of gratings. The standard fiber Bragg grating (SFBG), which is the simplest type of fiber grating, and the tilted optical fiber Bragg grating (TOFBG), which we use for the development of our chemosensor.

A SFBG consists of a periodic, uniform, modulation of the refractive index in the core of a SMF, where the phase fronts are perpendicular to the fiber's longitudinal axis with grating planes having constant period. Light guided along the core of an

optical fiber will be scattered by each grating plane. If the Bragg condition (energy-momentum conservation for the incident and the reflected radiation) is not satisfied, the reflected light from each of the subsequent planes becomes progressively out ofphase and will eventually cancel out. Where the Bragg condition is satisfied the contributions of reflected light from each grating plane add constructively in the backward direction to form a back-reflected peak with a centre wavelength defined by the grating parameters [37].

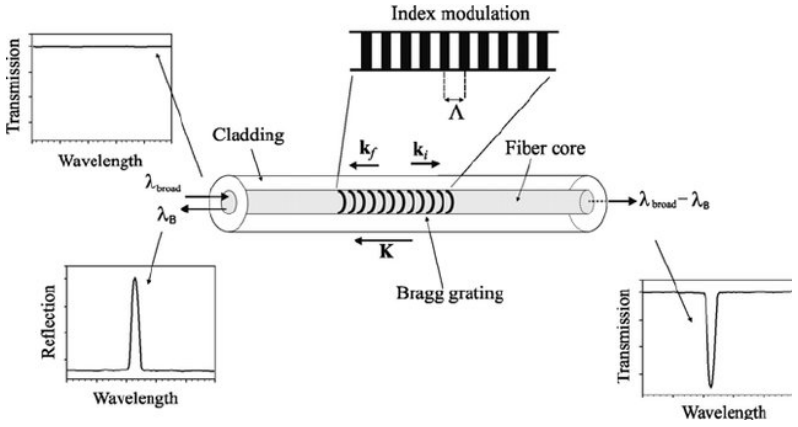

FIGURE 2.3: Illustration of a uniform Bragg grating with constant index of modulation amplitude and period. Also shown are the incident, diffracted, and grating wave vectors that have to be matched for momentum conservation. When the Bragg condition is satisfied a peak forms in transmission and a deep in reflection [37]

.

By tilting the grating planes relative to the perpendicular of the fiber axis, more complex interactions can be observed as light from the core can be guided to the cladding giving birth to new modes.

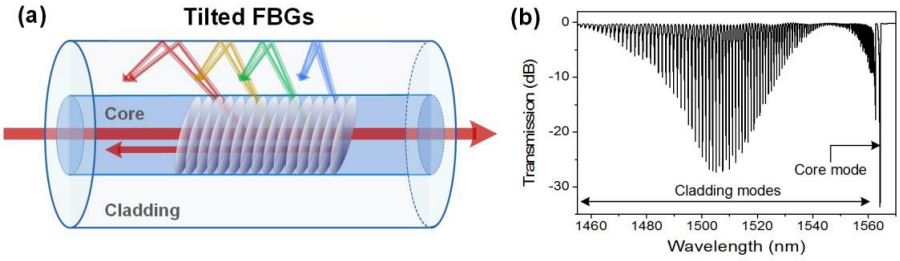

FIGURE 2.4: (a) Sketch of the light mode coupling in a tilted-fiber Bragg grating (TOFBG); and (b) transmitted amplitude spectrum [38]

.

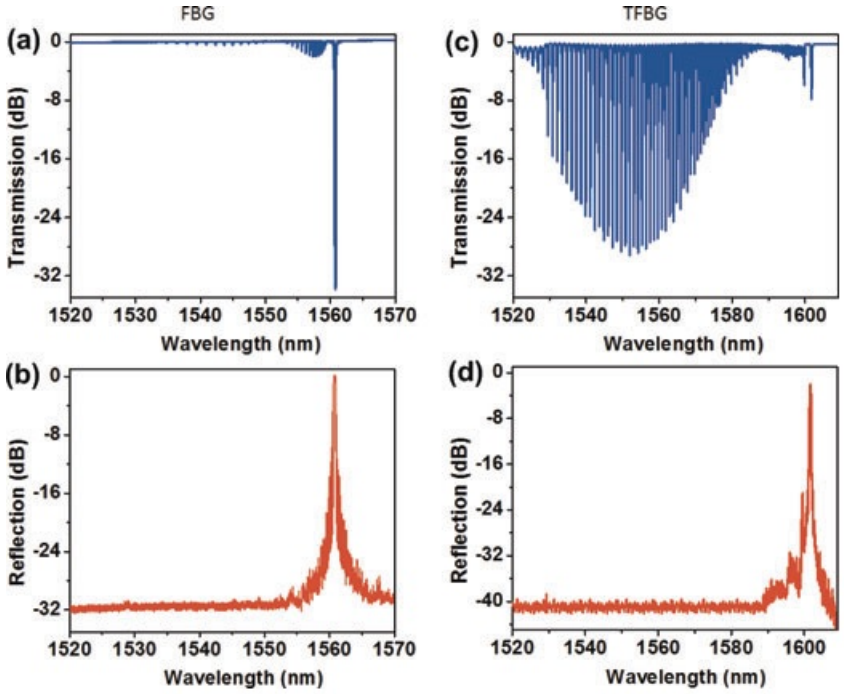

FIGURE 2.5: Transmission and reflection spectra for a SFBG [(a), (b)] and a TOFBG [(c), (d)] [39]

.

As seen in Fig.(2.5) normal FBG has only one strong resonance, i. e. a deep in transmission at the wavelength that satisfies the Bragg condition for this grating period in that particular fiber and the same resonance also appears as a single peak in the reflection spectrum. In addition to the Bragg resonance, the FBG spectrum has a large number of additional weak resonances but only in transmission. These

resonances arise from coupling to modes guided by the cladding and they do not show up in reflection because the power carried by these modes gets stripped away by the losses. When the grating planes are tilted we have a strong enhancement of the cladding mode resonances, at the expense of the Bragg resonance. The closest resonance to the Bragg (or fundamental) mode, which is usually stronger than its cladding mode neighbours on the short wavelength side, is called the "ghost" mode resonance and consists of the superposition of several low order cladding modes. Near 1530 nm in the TOFBG transmission spectrum there is a discontinuity in the cladding mode envelope after which (towards short wavelengths) the resonance amplitudes decrease sharply. This is due to a transition from guided cladding modes to leaky cladding modes (i. e. cladding modes with effective indices lower than the external medium). We observe also that the strongly resonant cladding modes of the TOFBG are not present in the reflection spectrum. This is because the tilted fringes of the grating front-scatter light into the cladding rather than reflect it, so not much of them can be observed in reflection[39].

2.2.1.1 Coupled mode theory for fiber gratings

Coupled-mode theory is perturbational theory that allows us to model complex vibrational systems as series of resonators that are coupled to one another in some way. Coupled-mode theory can be used with a wide variety of geometries or heteromaterials and has been used to analyze periodic structures or a small isolated surface dent or defect [40].

Thus, we use coupled-mode theory to describe gratings and the resonances they produce. A brief analysis for the SFBG is presented below.

2.2.1.1.1 Standard fiber Bragg gratings

We will assume the following: 1) our fiber is weakly guiding, 2) there are no absorption loss and 3) the propagating modes do not couple with the TE and TM radiation modes.

We begin by writing the wave equation in cylindrical coordinates:

$$\frac{\partial^2\psi}{\partial r^2} + \frac{1}{r}\frac{\partial\psi}{\partial r} + \frac{1}{\phi^2}\frac{\partial^2\psi^2}{\partial\phi^2} + \frac{\partial^2\psi}{\partial z^2} + n_i^2 k^2 = 0 \tag{2.15}$$

where $n_i = n_1, n_2 = n_{co}, n_{cl}$, ψ are scalar longitudinal fields and $k = 2\pi/\lambda$.

We will assume that:

$$\psi(r, \phi, z, t) = F(r)cos(\nu\phi)exp[i(\omega t - \beta z)] \tag{2.16}$$

and that n_i is uniform along z. By substituting eq.(2.15) to eq.(2.14), gives us the eigen fields : $\mathcal{E}_\nu$ and $\mathcal{H}_\nu$.

We assume that the SFBG refractive index profile is:

$$\epsilon(z) = \begin{cases} n_o^2 + \Delta\epsilon cos(\theta z) & \text{in core region} \\ n_o^2 & \text{in cladding} \end{cases} \tag{2.17}$$

where n_o is the refractive index of a uniform fiber, $\Delta\epsilon$ is the induced index perturbation, $\theta = 2\pi/\Lambda$ and Λ is the period of the grating. The perturbed fields of the grating are then expanded as:

$$E = \sum_{\nu=1}^{N} a_\nu \mathcal{E}_\nu \tag{2.18}$$

$$H = \sum_{\nu=1}^{N} b_\nu \mathcal{H}_\nu \tag{2.19}$$

where a_ν and b_ν are the mode amplitudes and N is the number of modes in the fiber. Eqs.(2.16), (2.17) and (2.18) are substituted to eq.(2.14). Assuming that higher harmonics are negligible and that transverse coupling coefficient is (Ω) is much larger than the longitudinal coupling coefficient, we get as a result:

$$\frac{dC_\mu^+}{dz} = \frac{\Omega}{i} C_\mu^- exp(i2\Delta\beta z) \tag{2.20}$$

$$\frac{dC_\mu^-}{dz} = \frac{\Omega}{i} C_\mu^+ exp(-i2\Delta\beta z) \tag{2.21}$$

where "+" is used to denote forward and "-" is used to denote backward traveling waves, $\Delta\beta = \beta - (\pi/\Lambda)$ and C_μ^- and C_μ^+ are the normalized amplitudes of the fields. Solving this pair of coupled differential equations using the boundary conditions $C^+(0) = 1$ and $C^-(L) = 0$, where L is the length of the SFBG, gives:

$$C^+(z) = \frac{-exp(i2\Delta\beta z)}{[\Delta\beta sinh(SL) - iScosh(SL)]}[\Delta\beta sinh(S(z-L)) + iScosh(S(z-L))] \tag{2.22}$$

$$C^{-}(z) = \frac{\Omega exp(-i2\Delta\beta z)}{[sinh(SL) - iScosh(SL)]} sinh(S(z-L)) \tag{2.23}$$

where $S = (\Omega^2 - \Delta\beta^2)^{1/2}$. From eqs.(2.21) and (2.22) we can get the reflectance and the transmittance as a function of wavelength.

$$R(\lambda) = \|C^{-}(0)/C^{+}(0)\|^2 \tag{2.24}$$

$$T(\lambda) = \|C^{+}(L)/C^{+}(0)\|^2 \tag{2.25}$$

We give the reflectance:

$$R(\lambda) = \begin{cases} \frac{\Omega^2 sinh^2(SL)}{[\Delta\beta^2 sinh^2(SL) + S^2 cosh^2(SL)]} & \text{for } \Omega^2 > \Delta\beta^2 \\ \frac{\Omega^2 sin^2(iSL)}{[\Delta\beta^2 - \Omega^2 cos^2(iSL)]} & \text{for } \Omega^2 < \Delta\beta^2 \end{cases} \tag{2.26}$$

Of course if we plot $R(\lambda)$ we will get the Bragg peak for the SFBG [41].

While an analytic result, that simulates reality to an acceptable degree, is possible with SFBGs the same cannot be said for TOFBGs. The complexity arises from the fact that if one wishes to simulate a spectrum that corresponds to reality even in the slightest, coupling with the radiation modes cannot be ignored. Furthermore, an accurate picture can be acquired only if one takes into consideration the cross-coupling of the radiation modes with other radiation modes. It is obvious that this problem, from a mathematical standpoint, is too complicated to be tackled analytically. Complex simulations must be done to produce a satisfying result.

Chapter 3

Experimental

3.1 Properties of SMF-28 optical fiber

For the development of our sensor SMF-28^{TM} optical fiber was used exclusively as its main platform. SMF-28^{TM} is a step-index SMF developed by Corning®. Specifically, this optical fiber consists of fused silica cladding enveloping a GeO_2 doped silica core. The GeO_2 doping contributes in raising the refractive index of the core. The GeO_2 doping also contributes in the SMF-28^{TM}'s photosensitivity in the core, due to the GeO_2 defects' large absorbance at 193 nm, a crucial characteristic in grating fabrication, as it will be discussed below.

Properties of SMF-28^{TM}	
Core Diameter	8.2 μm
Cladding Diameter	$\sim$ 125 μm
Refractive Index Difference	0.36%
Effective Group Index of Refraction	1.4682 at 1550 nm
Mode-field Diameter	10.4 $\pm$0.8 μm at 1550 nm
Cutoff Wavelength (λ_{cf})	$\lambda_{cf} \leq$ 1260 nm
GeO_2-Core Doping Levels	$\sim$3.6 mol %

FIGURE 3.1: Physical and optical properties of SMF-28 ^{TM}[42][43]

3.2 Grating fabrication

There are numerous methods to fabricate FBGs in silicate glass optical fibers. The most convenient and widely used method, adopted by the industry, is the phase mask technique. This method employs a diffractive optical element (phase mask) to spatially modulate the UV writing beam. Phase masks may be formed holographically or by electron-beam lithography. The phase mask grating has a one-dimensional surface-relief structure fabricated in a high quality fused silica flat transparent to the UV writing beam. The profile of the periodic surface-relief gratings is chosen such that when a UV beam is incident on the phase mask, the zero-order diffracted beam is suppressed to less than a few percent (typically less than 5%) of the transmitted power. In addition, the diffracted plus and minus first orders are maximized each containing typically more than 35% of the transmitted power. A near field fringe pattern is produced by the interference of the plus and minus first-order diffracted beams. This near field interference fringes is half of that of the period of the phase mask, while exploiting photosensitivity effects. The interference pattern photo-imprints a refractive index modulation into the core of an optical fiber placed in contact with or in close proximity immediately behind the phase mask. A cylindrical lens may be used to focus the fringe pattern along the fiber core.

The phase mask greatly reduces the complexity of the fiber grating fabrication system. The simplicity of using only one optical element provides a robust and inherently stable method for reproducing fiber Bragg gratings. Since the fiber is usually placed directly behind the phase mask in the near field of the diffracting UV beams, sensitivity to mechanical vibrations and therefore stability problems are minimized.

KrF excimer lasers are common UV sources used to fabricate Bragg gratings with a phase mask. These UV laser sources typically have low spatial and temporal coherence. The low spatial coherence requires the fiber to be placed in near contact to the grating corrugations on the phase mask in order to induce maximum modulation in the index of refraction. The further the fiber is placed from the phase mask, the lower the induced index modulation, resulting in lower reflectivity Bragg gratings. It should also be noted that if the zeroth order beam is not significantly suppressed,

interference will occur between 0th- and 1st-order diffracted beams; in this case the interference pattern will change as a function of the fiber-phase mask separation resulting in fringes that vary from half the phase-mask period to one period of the mask [44].

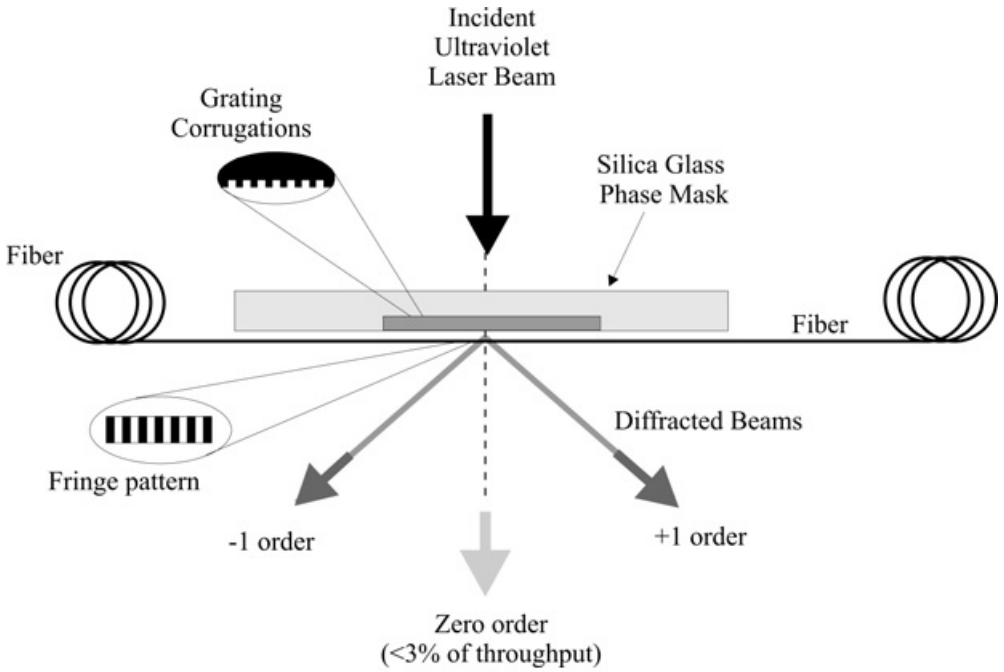

FIGURE 3.2: Phase-mask geometry for inscribing Bragg gratings in optical fibers[44]

3.2.1 Setup and process

In this section, the grating fabrication setup used and the inscription process, is described. For the grating fabrication, an ATLEX 300 FBG ArF Excimer Laser from ATL Lasertechnik, is employed. This pulse laser operates at 193 nm providing us with sufficient photon energy so to access defects near the Urbach tail of high transparency silicate glasses and inscribe gratings FBGs even at SMF-28 fibers.

The laser beam reaches the phase mask grating recording setup using two 45 degrees dielectric mirrors. Right after the second mirror an attenuator is placed. The attenuator is used to tune the power of the laser pulses for not damaging the phase mask. Then, a cylindrical lens focuses the beam through a diaphragm which is used

to apodize the beam before reaching the phase mask (of periodicity, $\Lambda_{pm} = 1070$ nm).

The SMF-28 is mounted on two magnetic fiber holders at a very small distance behind the phase mask. The area of the fiber that is right behind the phase mask is striped off its buffer and cleaned with isopropanol. Using fiber adaptors, one end of the fiber is connected directly with an optical spectrum analyser (A16317B OSA by Ando Electric Co Ltd) while the other is connected via a 50/50 coupler with an Erbium-doped Fiber Amplifier (EDFA) light source. Using the OSA, one can monitor the grating fabrication process online.

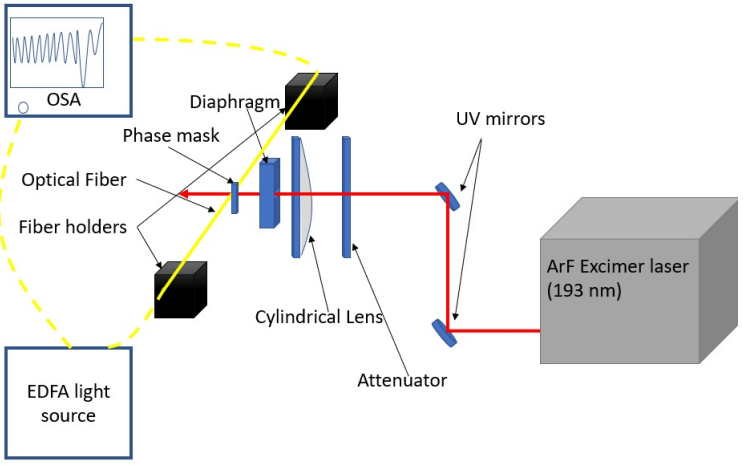

FIGURE 3.3: Schematic of the Bragg grating fabrication setup

To write a TOFBG, a small tilt is introduced between the fiber and the phase mask. In our case, a 3 degrees tilt is introduced between the phase mask and the optical fiber, since greater tilting angles result in a low extinction ratio fundamental mode in reflection. The fiber is irradiated at 40 Hz with pulses of 100 mJ/cm^2 energy density. Irradiation lasts for 30 minutes.

3.2.2 Spectral characterisation of the Bragg grating

In this section, is presented the spectrum of an inscribed TOFBG in a SMF-28 using the setup and conditions described above. After the inscription, the TOFBG's spectrum is scanned from 1530-1555 nm, using the OSA. The collected spectrum is saved and analysed.

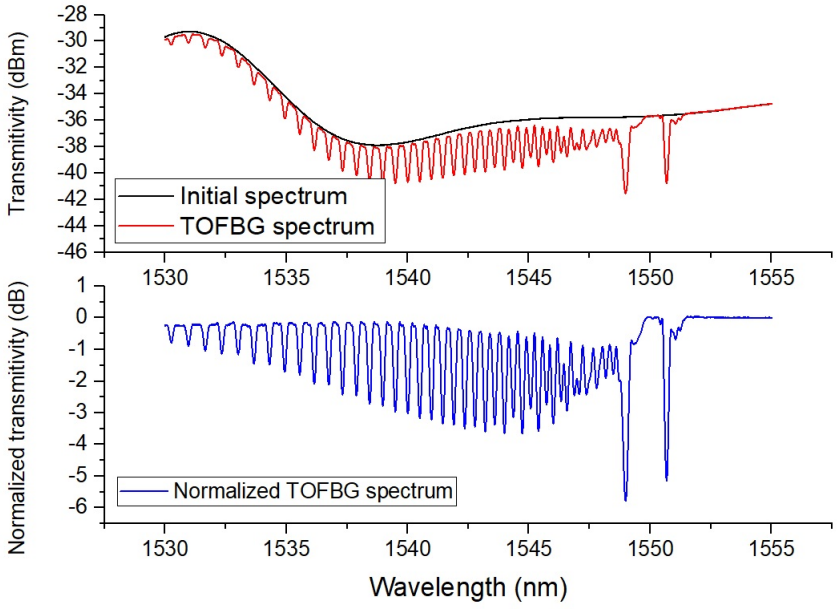

FIGURE 3.4: Spectra before and after inscription of a TOFBG in an SMF-28. The black line is the transmission spectrum of our light source. The red line shows the transmission spectrum after irradiating our fiber for 30 minutes.The blue line shows the normalized transmission spectrum of a TOFBG.

The fundamental mode (Bragg peak), for this specific grating, is found to be at 1550.676 nm, the ghost mode peak is at 1548.984 nm, while from 1548.478 to 1530 nm numerous cladding modes can be observed (at room temperature for zero applied strain).

3.3 Post-inscription processing of TOFBGs

In this section, the various post-inscription processes the TOFBG undergoes towards their implementation as chemosensing probes, are presented. Namely, the TOFBG is tempered, overlaid with P(VDF-TrFE-CTFE) polymer and annealed to remove the solvent. This leaves us with a TOFBG overlaid with amorphous P(VDF-TrFE-CTFE) polymer which can be used for measurements. Next, depending on whether one wants to study the crystalline or the thermally poled state of P(VDF-TrFE-CTFE) polymer, further processing of P(VDF-TrFE-CTFE) polymer overlaid TOFBG is carried out. To improve the film crystallinity additional annealing processing steps are

introduced; similarly, thermal poling is carried out-using a different volto-annealing process.

3.3.1 Thermal tempering

As it was discussed above, grating fabrication is possible due to the fiber's core photosensitivity to UV radiation. When a fiber is irradiated with UV light, structural defects (color centers) are created in the fibers crystal lattice. Transformation of colour center defects takes place into the amorphous glass matrix, which in turn are translated to refractive index/loss changes. However, not all of these defects are thermally stable, meaning that when the grating is thermally annealed some of these defects will vanish, resulting in permanent changes to its spectral characteristics. The first step for developing the sensor presented herein, is a thermal tempering process, so to remove refractive index demarcation effects that will be convoluted with the behaviour of the P(VDF-TrFE-CTFE) polymer during its casting and annealing process, allowing us a precise study of the P(VDF-TrFE-CTFE) thin film casting process.

This can be done by simply heating our grating at a high temperature. Specifically, our gratings are annealed at 250 °C for 1 hour. This temperature is chosen as it is at least two times higher than any other temperature that is used during the various post-inscription processes.

3.3.2 P(VDF-TrFE-CTFE) polymer overlaying of TOFBG

After tempering, the TOFBG is overlaid with a P(VDF-TrFE-CTFE) polymer film. A solution of P(VDF-TrFE-CTFE) dissolved in cyclopentanone (2.5% w/w) is spread on the grating. At the same time the grating is annealed at 70 °C as to solidify the polymer as quickly as possible. Cyclopentanone by itself is considerably volatile so after a few minutes the polymer film becomes solid. After that, the grating is cased inside a small bronze kiln and is annealed at 70 °C for another 1 hour to completely evaporate the solvent. After that, the grating is removed from the kiln and is let to rest. Spectra are collected to determine the changes the P(VDF-TrFE-CTFE) polymer film introduces.

At this stage, the P(VDF-TrFE-CTFE) polymer film is in its amorphous state. The P(VDF-TrFE-CTFE) overlaid grating could be used for sensing in our experiments with the perfluorinated substances. So, tempering, overlaying and thermally annealing to remove the solvent consists of the bare minimum of processing our sample must undergo to produce a functioning sensor.

Below, we present SEM images of a The P(VDF-TrFE-CTFE) overlaid fiber that has been vertically cleaved, in order to get an estimate of the polymer film's thickness. Using an image processing software, one can get a pretty accurate approximation of the polymers thickness. Close-up images of different points of the fiber were taken. The thickness, for this sample, is found to be between 2.5 and 4.2 μm. Because the overlaying process is done manually, the polymer film thickness tends to be considerably inconsistent, not only between two different overlaid fibers but between to different points on the same fiber.

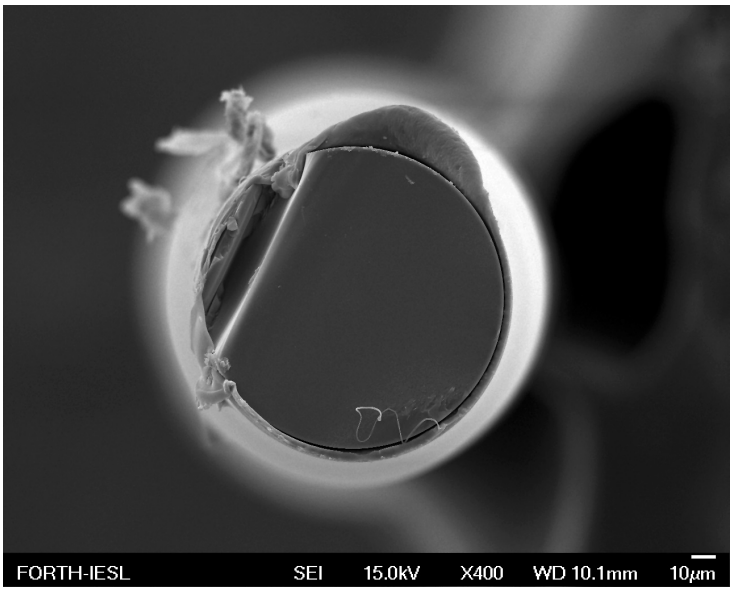

FIGURE 3.5: Vertically cleaved, polymer overlaid fiber.

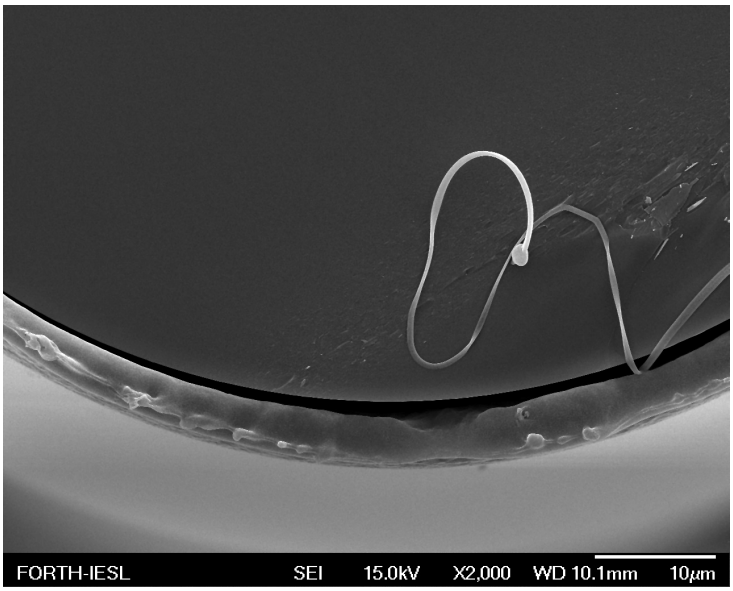

FIGURE 3.6: Close-up image of the south side of the fiber. The thickness of the polymer film was found to be between 3.4 and 4.2 μm.

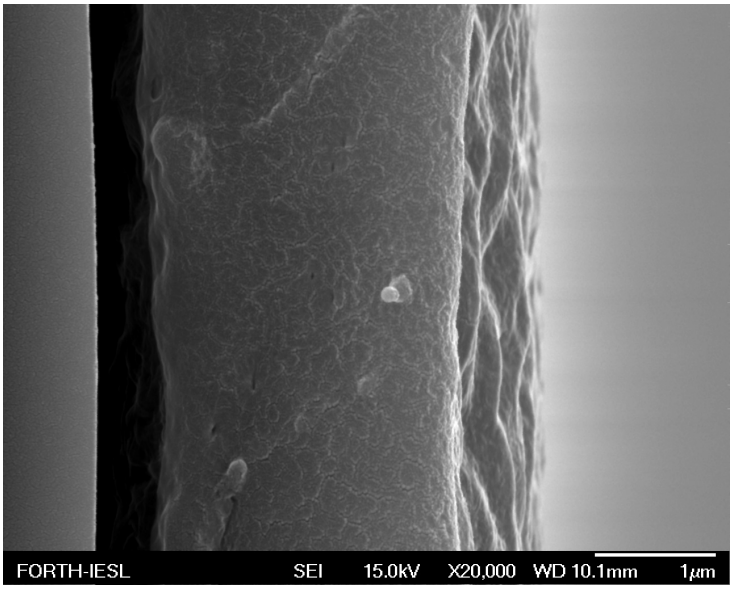

FIGURE 3.7: Close-up image of the right side of the fiber. The thickness of the polymer film was found to be $\sim$2.5μm

3.3.3 Annealing of P(VDF-TrFE-CTFE) polymer overlaid TOFBG

To study the response of the crystalline phase, the P(VDF-TrFE-CTFE) overlaid TOFBG is placed back on the kiln and raise the temperature up to 130 °C. At 120 °C P(VDF-TrFE-CTFE) is in its melt phase, meaning that any crystal formations in the film due

to the previous thermal treatments are erased. Our sample is let to anneal for 15 minutes at 130 °C, then the temperature is slowly dropped to 110 °C, which is the temperature at which maximum crystallization occurs, and leave the grating for 1 hour to anneal. After 1 hour, the grating is removed from the kiln while the heat is still on. This is done in order for the polymer film to cool instantly, "freezing" the polymer in the induced crystalline state. Spectra are collected to determine the changes annealing introduces.

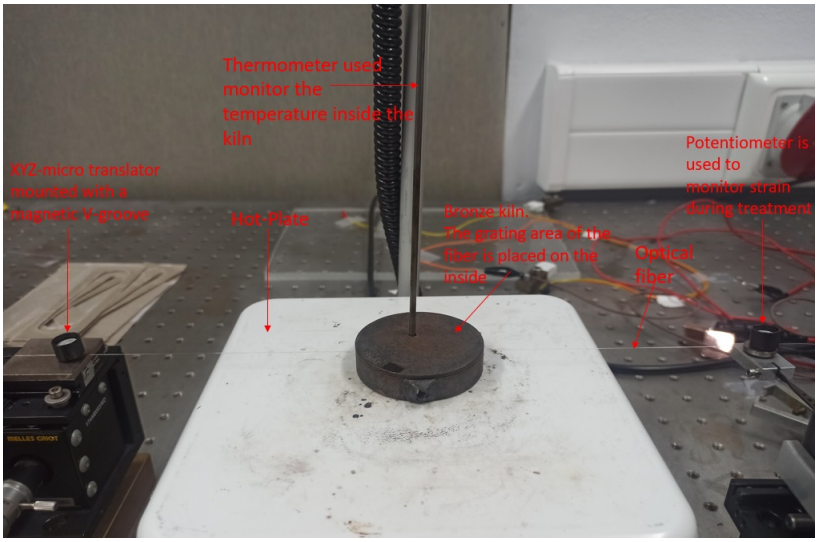

FIGURE 3.8: Experimental setup used for tempering the TOFBGs and annealing the P(VDF-TrFE-CTFE) overlaid gratings.

3.3.4 Thermal poling of the P(VDF-TrFE-CTFE) overlaid TOFBG

To induce a polarization in the polymer film, the overlaid grating is placed between two copper-covered steel electrodes. The electrodes are connected to high voltage generator that is able to supply us with voltages up to 5000 V. The electrodes are placed on a hot-plate. The temperature is raised to 100 °C and turn on the voltage generator.The voltage is raised up to 2000 V, right before breakdown occurs. The induced electric field is calculated to be 8 MV/m. The sample is left to pole for 1 hour at maximum voltage. After 1 hour, the hot-plate is turned off and the system is let to slowly cool-down with the voltage still on. This is done in order to make sure that the induced polarization is not lost due to the high temperature. When the

temperature drops to room temperature the voltage is turned off and the sample is removed . Again, spectra of the thermally poled sample, are collected.

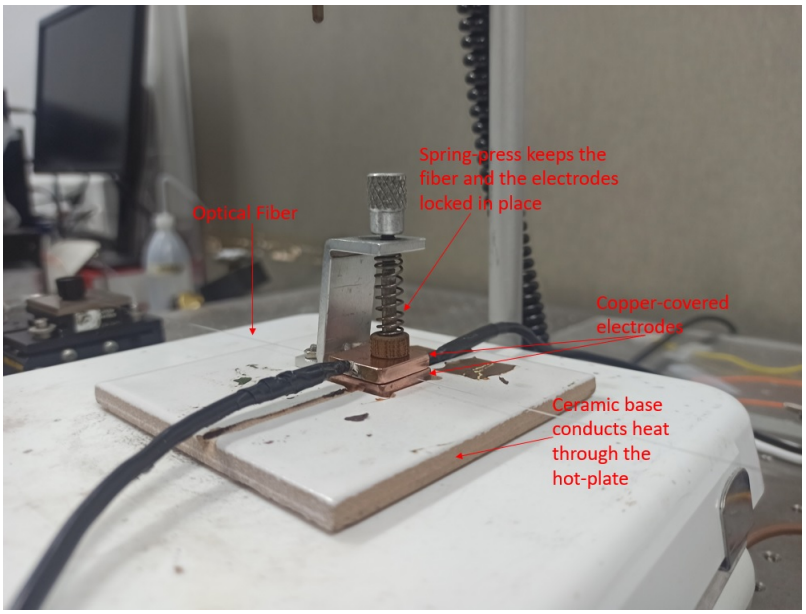

FIGURE 3.9: Experimental setup used to pole P(VDF-TrFE-CTFE) overlaid gratings.

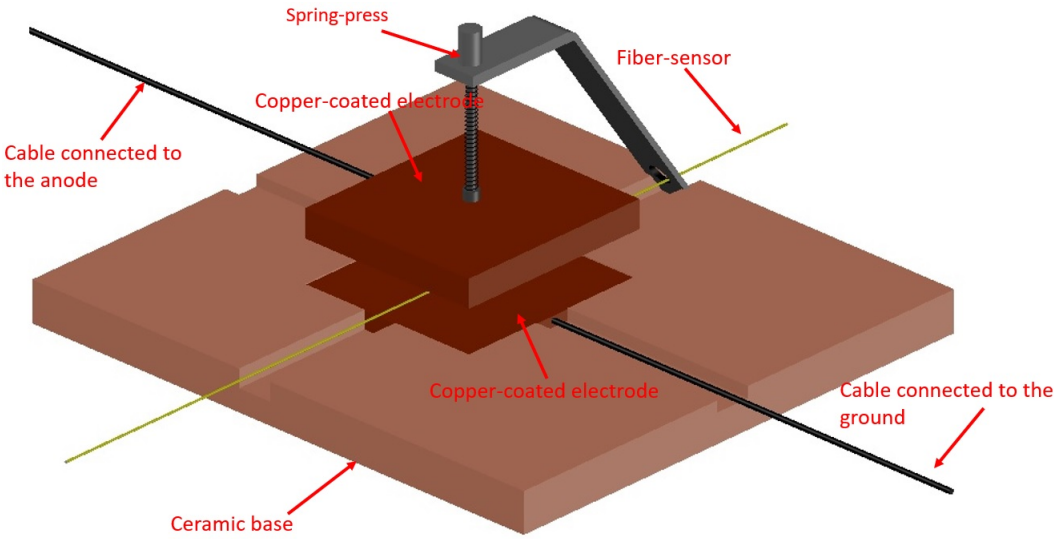

FIGURE 3.10: Diagram of the experimental setup depicted in Fig.(3.9).

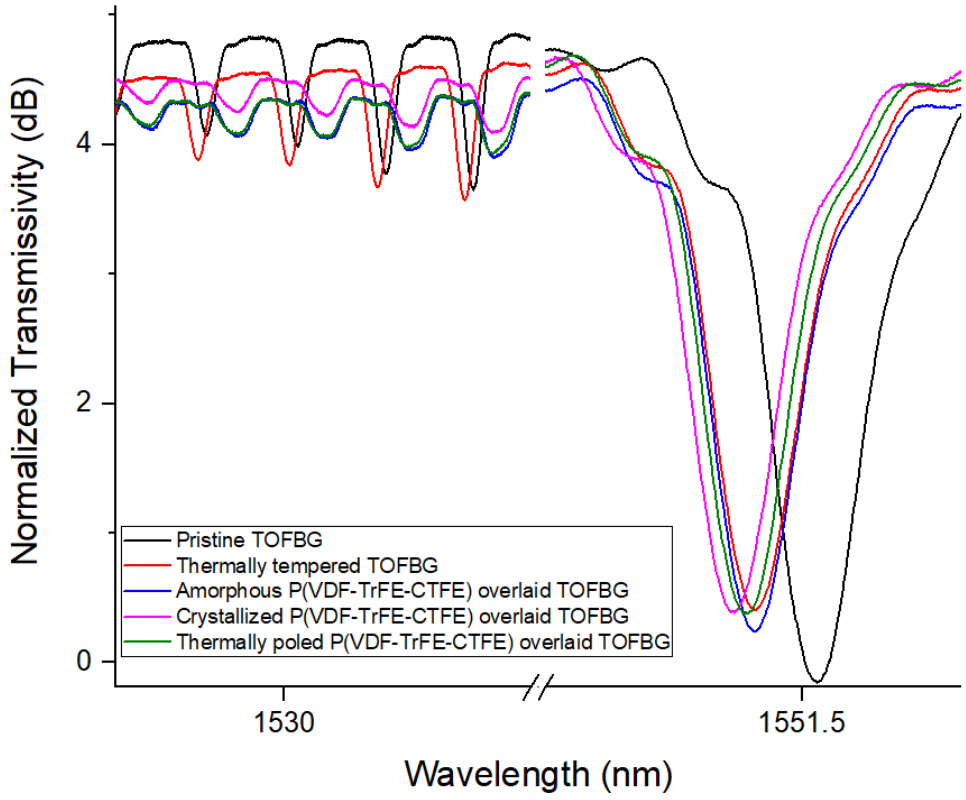

FIGURE 3.11: Transmission spectra of a grating's fundamental and cladding modes after different post-inscription processes.

Spectral shifts ($\Delta\lambda$) between different TOFBG treatments		
	($\Delta\lambda$) of the fundamental mode (nm)	**($\Delta\lambda$) cladding mode ($\sim$1530 nm) (nm)**
Pristine→Thermally Tempered	-0.12	-0.064
Tempered→P(VDF-TrFE-CTFE) overlaid	0	+0.302
P(VDF-TrFE-CTFE) overlaid→Crystallized	-0.042	-0.006
Crystallized→Thermally Poled	+0.022	+0.014

FIGURE 3.12: Spectral shifts between different post-inscription processes.

In Fig.(3.11) one sees the spectral shifts and intensity changes of the fundamental and cladding modes of a grating that has undergone different treatments. In Fig.(3.12), the values of the spectral shifts are presented for the grating depicted in Fig.(3.11). It should be noted that these values are typical and not absolute, meaning that they slightly change from grating to grating.

The elimination of the thermally unstable defects during tempering has both lowered the intensity of the fundamental and cladding modes but also shifted our spectra towards the blue.

When the tempered grating was overlaid with the polymer minimal changes on the fundamental mode were observed, while the cladding modes shifted significantly towards red. This is to be expected, as the addition of the polymer around the fiber increases the effective refractive index around the cladding resulting in a shift towards greater wavelengths for the cladding modes. However, as the core is away from cladding-environment interface, the fundamental mode remains unchanged.

When annealing takes place, the fundamental and the cladding modes shift towards blue in comparison with the overlaid grating. This is most likely because the polymer solidifies and mechanically compresses the grating.

Finally, a poled grating seems to drift towards red for both the core and the cladding modes in relation to the annealed grating. There are several reasons for this: 1) the change of the orientation of the electric dipoles of the polymer induces a change on the refractive index, 2) as the polymer is electrostrictive, the induced polarization induces a mechanical strain on the grating or 3) a combination of the phenomena occurs.

3.4 Experimental apparatus and process

In this section, the experimental setups and the experimental process followed to test our sensors sensitivity to perfluorinated chemicals, is described. Two setups were used: one to test sensitivity to gaseous chemicals and one to test sensitivity to aqueous solutions.

3.4.1 Experimental setup: sensing of TFE vapors

To test our sensor's sensitivity to perfluorinated gases a gas chamber is needed. Our gas chamber consists of a stainless steel cylindrical container which has been drilled on its sides so that an optical fiber be threaded through the container. A plexiglass lid seals the container from above, held in place by eight screws. The container has two gas inlets and one gas outlet. One gas inlet is connected to a nitrogen tank while the other is placed on top of the plexiglass lid and is used to add chemicals inside the chamber. A manometer is also connected with the chamber in order to monitor pressure.

Our experiment begins by placing the treated grating in the chamber. The two ends of the fiber are connected to the OSA, in order to monitor the transmission spectrum online. The chamber is sealed and an initial spectrum of our sensor is collected, to be used as a reference. Next, liquid trifluoroethanol (TFE) is added in the chamber. As the liquid evaporates the pressure rises. Spectra were collected every 5 minutes for up to 2 hours. After 2 hours, the gas outlet is opened to release the gas. The gas inlet connected to the nitrogen tank is opened and, with the outlet open, the nitrogen is let to flow through the chamber. The nitrogen inflow remains open for 10 minutes to flush all of TFE off the chamber. After 10 minutes of flushing, the outlet

is closed to let the gas chamber to fill with nitrogen gas. Spectra are collected every 5 minutes for 1 hour with our sensor inside the nitrogen atmosphere. This is done to study our sensors behaviour when the measurand is removed. After 1 hour passes the gas outlet is opened to release pressure and remove our sensor off the chamber.

In order to remove any TFE that may be absorbed in the polymer film, the grating is annealed at 130 °C for 15 minutes. After that, the sensor is used again for more measurements. Data for multiple concentrations of TFE are gathered.

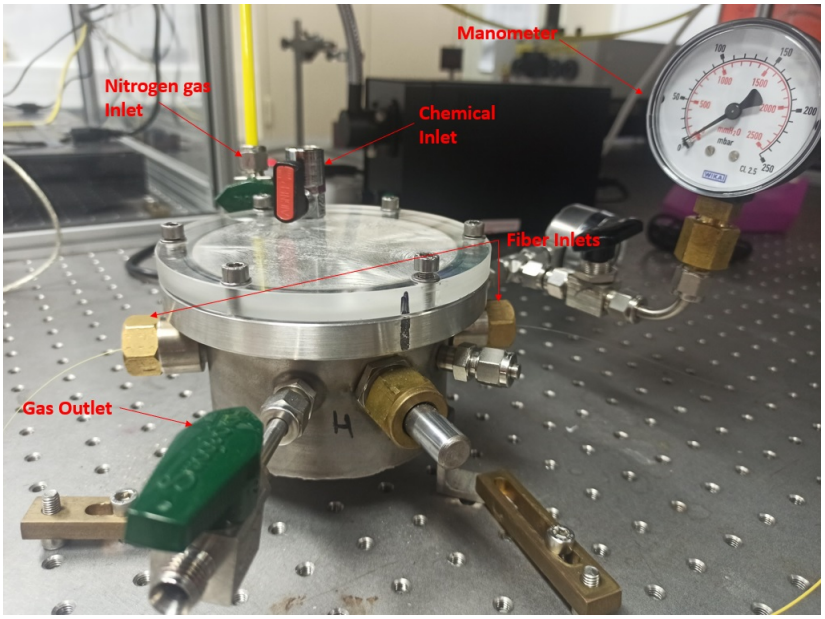

FIGURE 3.13: Experimental setup used to test our sensor's sensitivity to TFE vapors.

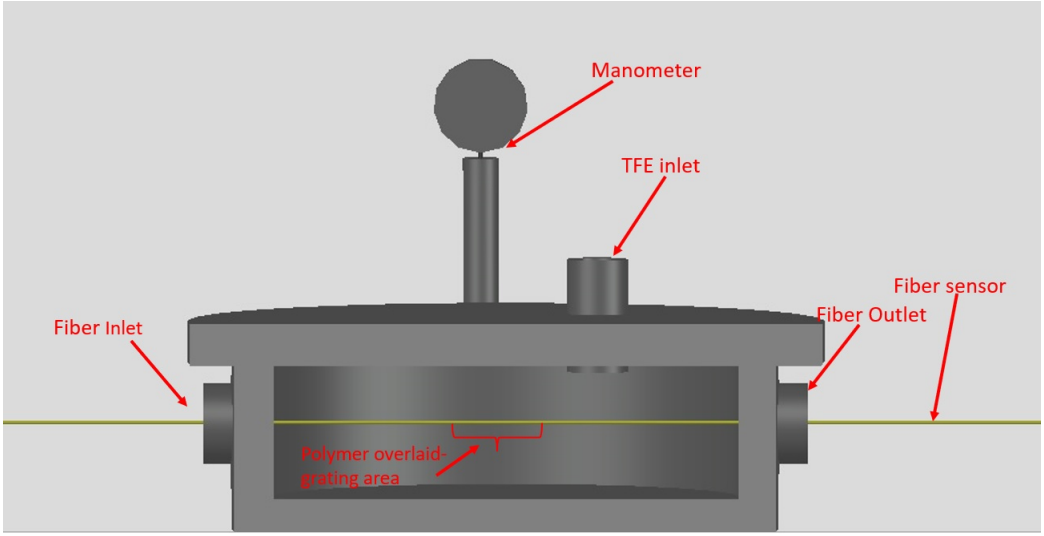

FIGURE 3.14: Diagram of the experimental setup depicted in Fig.(3.13).

3.4.2 Experimental setup: Perfluoroctanoic Acid (PFOA) sensing in aqueous solutions

PFOA was procured from Sigma-Aldritch Co. in solid form. A 100 ppm aqueous solution is created. By diluting this solution with more water smaller concentration solutions are created for our experiments.

The sensor is first suspended using one fiber holder and a potentiometer, leaving the P(VDF-TrFE-CTFE) overlaid grating area in the middle. The potentiometer is used to make sure that strain remains constant throughout our experiments. The two ends of the fiber are connected with the OSA in order to collect transmission spectra during the experiment. An initial spectrum of our grating is collected and will be used as a reference. A XZ-micro translator is placed right under the grating area. A microscope glass with some deionised water is placed on the XZ-translator. The XZ-translator is raised so that the water puddle that has formed on the microscope glass completely envelops the grating area. It is important to make sure that the glass surface does not come to contact with the grating as this will put extra strain on the grating.

With the grating submerged in the water puddle spectra are collected every 5 minutes for a total 40 minutes. This is done to condition our sensor in the solvent

(water) environment and to gather data in order to deconvolute the spectral changes due to the solvent from the ones due to the solute (PFOA).

After 40 minutes the microscope glass with the DI water, is removed from the XZ-translator. We place a new microscope glass with a aqueous solution of PFOA (data for multiple concentrations, are gathered). Data were gathered every 5 minutes for 40 minutes.

Finally, the microscope glass with the solution, is removed and a microscope glass with DI water is put in its place. This is done to clean our sensor from any PFOA residues. Again, data are gathered every 5 minutes for a total of 40 minutes.

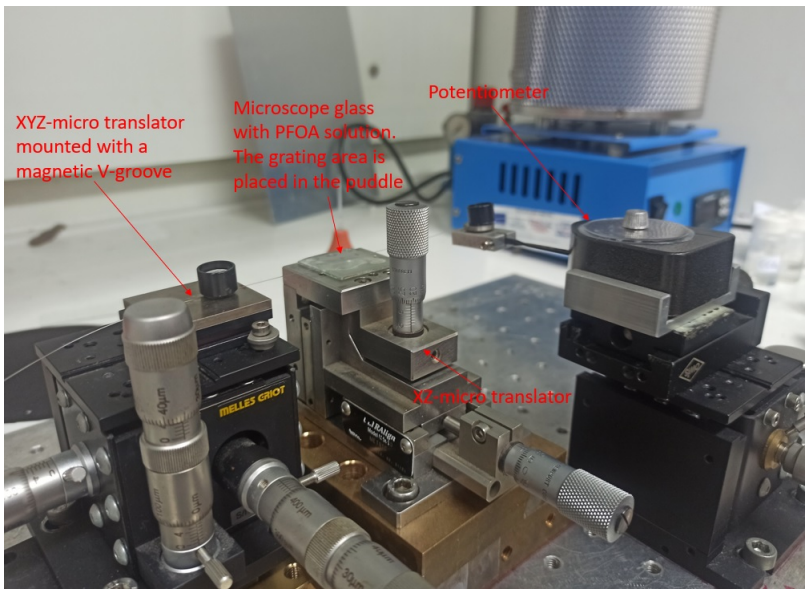

FIGURE 3.15: Experimental setup used to test our sensor's sensitivity to PFOA aqueous solutions.

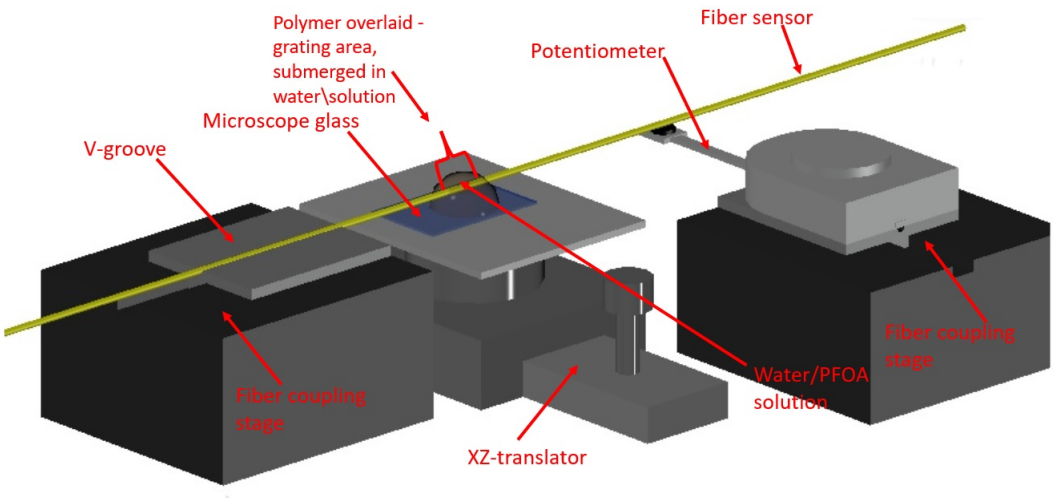

FIGURE 3.16: Diagram of the experimental setup depicted in Fig.(3.15) .

3.5 Properties and uses: P(VDF-TrFE-CTFE)

Polyvinylidene fluoride (PVDF), is part of the fluoropolymers family; a group of specialised, versatile polymeric materials with distinct properties that result from the strong bond between their carbon atoms and fluorine atoms and the fluorine shielding of the carbon backbone. PVDF is a specialty polymer with pyroelectric and piezoelectric properties and is used in the manufacturing of diverse high-purity, high-strength, and high-chemical-resistance products for applications in electrical, electronic, biomedical, construction, fluid-systems, oil-and-gas, and food industries.

PVDF is a semicrystalline, thermoplastic polymer. Its degree of crystallinity varies in the range of 35 - 70%, depending on the method of preparation. What makes it special is that it has a unique combination of mechanical and electrical properties (i.e., piezoelectricity), retains high standards of purity, and possesses high resistance to most chemicals including solvents, acids, and hydrocarbons.

There are five known crystalline forms in PVDF: alpha, beta, gamma, delta, and epsilon. The beta phase is the most commonly used form, and together with the alpha and gamma phases constitute the major phases.

The alpha phase is non-polar and is generated in the melting process from melt crystallisation at any temperature. The beta phase is an oriented phase that results

from the mechanical deformation of the specimen via uni-axial or bi-axial mechanical drawing below 70 °C. It is the most used for piezoelectric applications. The gamma phase is a special form that develops under specific circumstances. It can be generated through crystallisation at temperatures close to the melting point of the alpha phase via melt casting or solution casting [45].

The beta phase of PVDF has attracted much attention over the years and has been studied extensively due to the many applications of electroactive polymers. Namely, PVDF has been extensively applied in sensing and actuating (e.g. in acoustic emission monitoring, controlled displays, robots, artificial muscles) due to its inherent piezoelectric effect [46].

However, PVDF favors the alpha phase over all others due to its thermodynamic stability. In order to increase the beta phase and simultaneously reduce the crystallinity of the alpha phase, many methods have been developed during the preparation of PVDF materials. Copolymers of PVDF, such as P(VDF-TrFE), have been synthesized to achieve an intrinsic beta phase crystal while improving on the piezoelectric characteristics of PVDF. A lot of copolymers of PVDF have been synthesised over the years to both improve on the piezoelectric response and introduce certain desired characteristics on the polymer (e.g. greater elasticity or rigidity, transparency etc)[47][46].

By adding another "defect" on P(VDF-TrFE) a new copolymer has been created with ferroelectric relaxor rather than normal piezoelectric characteristics; the poly(vinylidenefluoride-trifluoroethylene– chlorotrifluoroethylene) terpolymer [P(VDF–TrFE–CTFE)] [48]. Relaxor ferroelectrics are materials that exhibit high electrostriction. Electrostriction is a mechanism that all materials possess and it consists of a mechanical displacement as a response to an electric field. The main differences between electrostriction and piezoelectricity are that: for electrostriction strain-field relationship is squared, electrostriction distortion does not depend on the direction of the electric field and that all materials, not just some special crystal groups, exhibit it to some degree[49].

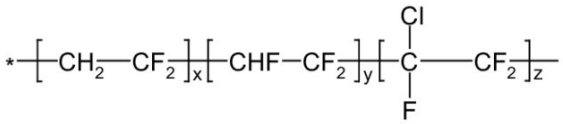

FIGURE 3.17: Chemical structure of P(VDF–TrFE–CTFE) [50].

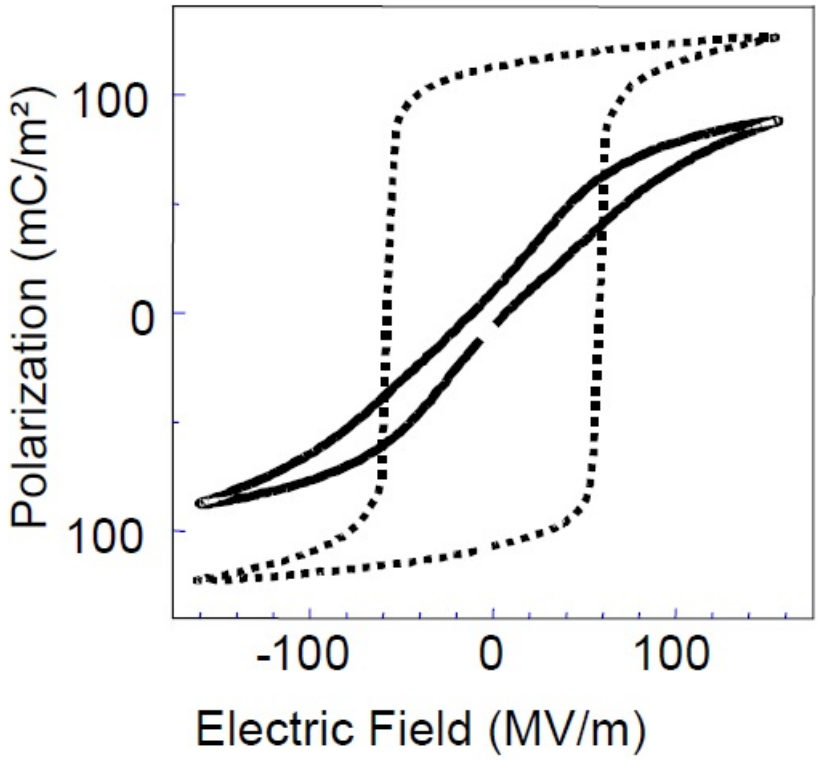

FIGURE 3.18: Comparison of the polarization hysteresis of the normal ferroelectric polymer (dashed curve, large hysteresis) and relaxor ferroelectric polymer (black curve, small hysteresis) at room temperature[51].

In our experiments, P(VDF–TrFE–CTFE) is used as a kind of "attractor" for the fluorinated substances we wish to sense. Fairuza Faiza et al. have reported that using a PVDF film on a fiber sensor can utilize the polymer's ferroelectric properties due to the presence of the beta or gamma phase in the polymer structure. The surface charge on PVDF can help in binding with PFOA in aqueous solution through dipole-dipole or hydrophobic interactions, since the contaminant has a carboxylate group that interacts strongly with polar substances and also an octyl group, which is inert

and hydrophobic [23]. The same can be inferred for P(VDF–TrFE–CTFE) and its interaction with PFOA as well as TFE.

Furthermore, we investigated the different response of our sensor depending on whether the P(VDF-TrFE-CTFE) film is in amorphous, crystalline or poled state. To establish at which temperature the P(VDF–TrFE–CTFE) film must be annealed for crystallization to occur differential scanning calorimetry (DSC) was used.

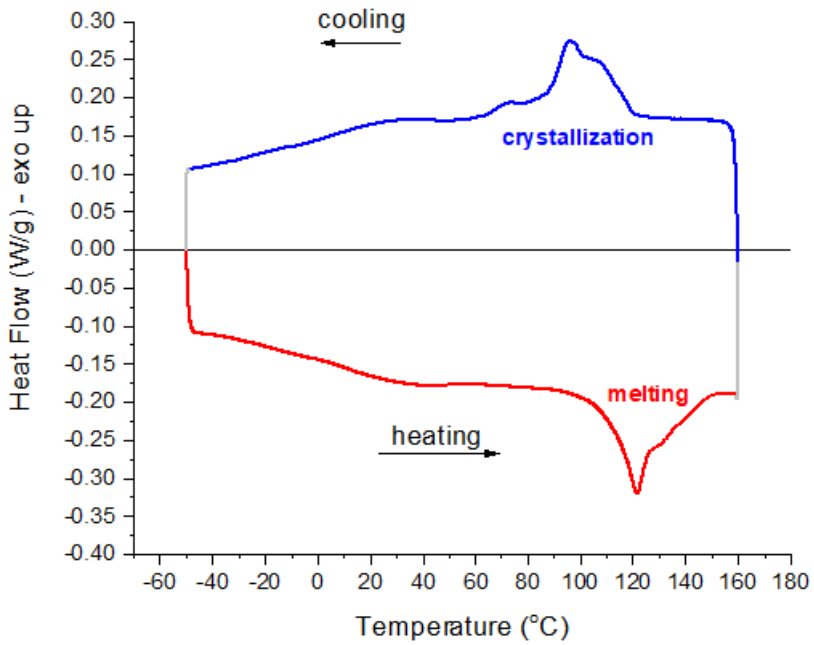

FIGURE 3.19: DSC curves for P(VDF–TrFE–CTFE).

From the DSC curves it is apparent that crystallization occurs during cooling between 100 and 110 °C, while melting occurs at 120 °C.

3.6 Properties and uses: 2,2,2-Trifluoroethanol (TFE)

TFE is one of the two fluorine compounds used to test our sensors sensitivity TFE is the organic compound with the formula CF_3CH_2OH. TFE is a colourless, water-miscible liquid that has a strong alcohol smell. Having a relatively low flash point, TFE tends to evaporate quickly off surfaces at room temperature. That is one of the reasons we chose TFE to test our sensors sensitivity to fluorinated gases.

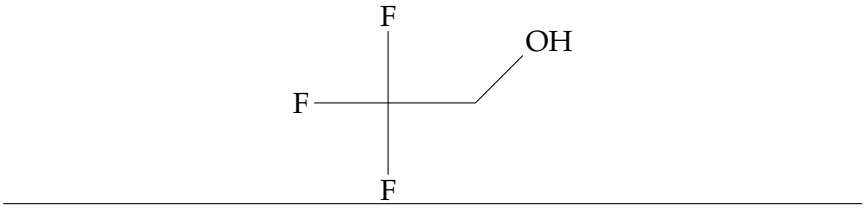

FIGURE 3.20: Chemical structure of TFE [52].

Properties	
Chemical formula	CF_3CH_2OH
Molar mass	100.04 g/mol
Density	1.3842 g/ml (at 20 °C)
Melting Point	-44 °C
Boiling Point	74 - 75 °C
Flash point	29 °C
Vapor Pressure	70 mm Hg (at 25 °C)
Refractive index	$n_{20/D}$=1.2907

FIGURE 3.21: Physical and chemical properties of TFE [53].

TFE is produced industrially by hydrogenation or the hydride reduction of derivatives of trifluoroacetic acid, such as the esters or acyl chloride [54].

TFE serves as a solvent and a raw material in organic chemistry and biology. TFE is a solvent of choice for hydrogen peroxide-mediated oxidations of sulfides. TFE acts as a protein denaturant. It is used in the manufacture of certain pharmaceuticals and drug substances[24]. Namely the drug Forane (Isoflurane), which is used for general anesthesia[25]. It is an effective solvent for peptides and proteins, and used for NMR-based protein folding studies, and in the manufacture of nylon. As a source of the trifluoromethyl group, it is employed in several organic reactions[24].

TFE's wide use in both industry and medicine births the need for real time monitoring of its concentration in both the atmosphere, for safety reasons, and, directly, in the field of application. This proves to be especially crucial in the field of medicine where imprecise dosology can render a substance from therapeutic to toxic.

3.7 Properties and uses: Perfluoroctanoic Acid (PFOA)

PFOA is the second perfluorinated chemical used to test the sensitivity of our sensor. PFOA is a completely fluorinated organic acid that is produced synthetically as its salts. It has the appearance of a white solid with a pungent odor. The typical structure has a nonbranched chain of eight carbon atoms ($C_8HF_{15}O_2$).

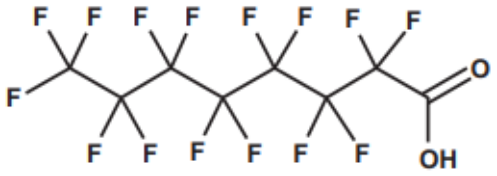

FIGURE 3.22: Chemical structure of PFOA [55].

Properties	
Chemical formula	$C_8HF_{15}O_2$
Molar mass	414,07 g/mol
Density	1,792 g/cm^3 (at 20 °C)
Melting Point	54.3 °C
Boiling Point	192.4 °C
Flash point	98.5 °C
Vapor Pressure	0.155 mmHg (at 25 °C)
Refractive index	$n_{20/D}$= 1.387
Solubility in water	3,4 g/l (at 20 °C)

FIGURE 3.23: Physical and chemical properties of PFOA [56] [57].

The industrial production of perfluoroalkyl carboxylates started in the late 1940s. Two principal production processes are used to manufacture PFOA, viz. electrochemical fluorination and telomerization. PFOA can also appear as a result of degradation of some precursors, e.g., fluorotelomer alcohols. The ammonium salt of

PFOA is primarily used as an emulsifier or 'processing aid' in industrial applications, for example, in the production of fluoropolymers such as polytetrafluoroethylene, but also produced for fluorosurfactant use. Typical uses include fluoropolymers in electronics, textiles, and nonstick cookware, and fluorosurfactants in aqueous filmforming foams used for fire fighting.

Like most industrial chemicals, when disposed, PFOA manages to find its way to an aquifer and from there infiltrate the rest of the environment. Once in the environment, PFOA is persistent and not known to undergo any further abiotic or biotic degradation under relevant environmental conditions. PFOA is highly water-soluble and typically present as an anion (conjugate base) in solution. It has low vapor pressure; therefore, the aquatic environment is expected to be its primary sink, with some additional partitioning to sediment. The presence of PFOA in the Arctic indicates the long-range transport of PFOA (e.g., via ocean currents) or of volatile precursors to PFOA (e.g., via atmospheric transport). Accumulation of PFOA in wildlife is much less than in humans.

Studies with animals fed PFOA for a long period showed effects on the stomach, liver, and thyroid hormones. Animal studies also indicate that PFOA may cause cancer at relatively high levels. PFOA has also been shown to be a developmental toxicant, and to have effects on the immune system. PFOA affects primarily the liver and can cause developmental and reproductive toxic effects at relatively low dose levels in experimental animals. It increases the tumor incidence in rats, mainly in the liver. The carcinogenic effects in rats appear to be due to indirect/nongenotoxic modes of action. Epidemiological studies in PFOA-exposed workers do not indicate an increased cancer risk. There is relatively consistent evidence of modest positive associations between serum levels of PFOA and cholesterol, uric acid, and liver enzyme levels[55].

The adverse effects of PFOA to human health and its constant bioaccumulation has raised much concern over the years. Monitoring water sources regularly to detect its concentration may prove crucial for the general public health. Furthermore, monitoring the concentration of PFOA in bodily fluids of cattle may give us some insight on how severely the food chain has been contaminated.

Chapter 4

Results and Discussion

4.1 TFE vapor sensing

In this section we discuss the results of our experiments using TFE vapors. Our sensor was exposed to different vapor pressures of TFE. Specifically, 1, 2, 5, 10 and 20 μl of TFE were dropped inside the gas chamber and let to evaporate. Knowing the gas chamber volume to be 0.5 litre, the ppm concentration ($\mu l/l$) is calculated to be 2 (for 1 μl), 4 (for 2 μl), 10 (for 5 μl), 20 (for 10μl) and 40 (for 20μl) ppm respectively. Using these concentrations, data for the P(VDF–TrFE–CTFE) polymer film in its amorphous phase and its crystalline phase, were collected. Data for the thermally poled phase were collected for the 2 ppm concentration. As discussed above, after each exposure our sample was let to rest for 1 hour in a nitrogen atmosphere before it was removed from the chamber and thermally annealed to 130 °C to remove any TFE residues. In the case of the crystalline sample, after each measurement the sample had to be annealed all over, as annealing at 130 °C renders the P(VDF–TrFE–CTFE) polymer film amorphous.

By using a spectrum of our sensor at equilibrium as a reference, spectral shifts versus time are calculated. To be precise, we measure the spectral shifts of the fundamental mode and a specific cladding mode (located at 1530.7 nm). This is done in order to determine the physical cause of these shifts. The results for the amorphous, the crystalline phase and the thermally poled phase are presented in the sections below.

4.1.1 TFE sensing using amorphous P(VDF–TrFE–CTFE) overlaid TOFBG

In Fig.(4.1) one can see the spectral shifts of the fundamental and the cladding mode versus time of the amorphous P(VDF–TrFE–CTFE) overlaid TOFBG probe. Fig.(4.1) shows that the fundamental and the cladding modes shift towards smaller wavelengths (blue shift). For the fundamental mode, which is spatially confined in the core of the fiber, this indicates that the fiber is subjected to mechanical strain when TFE interacts with the P(VDF–TrFE–CTFE) polymer transduction layer. For verification purposes the temperature was monitored during those measurements and found to be constant.

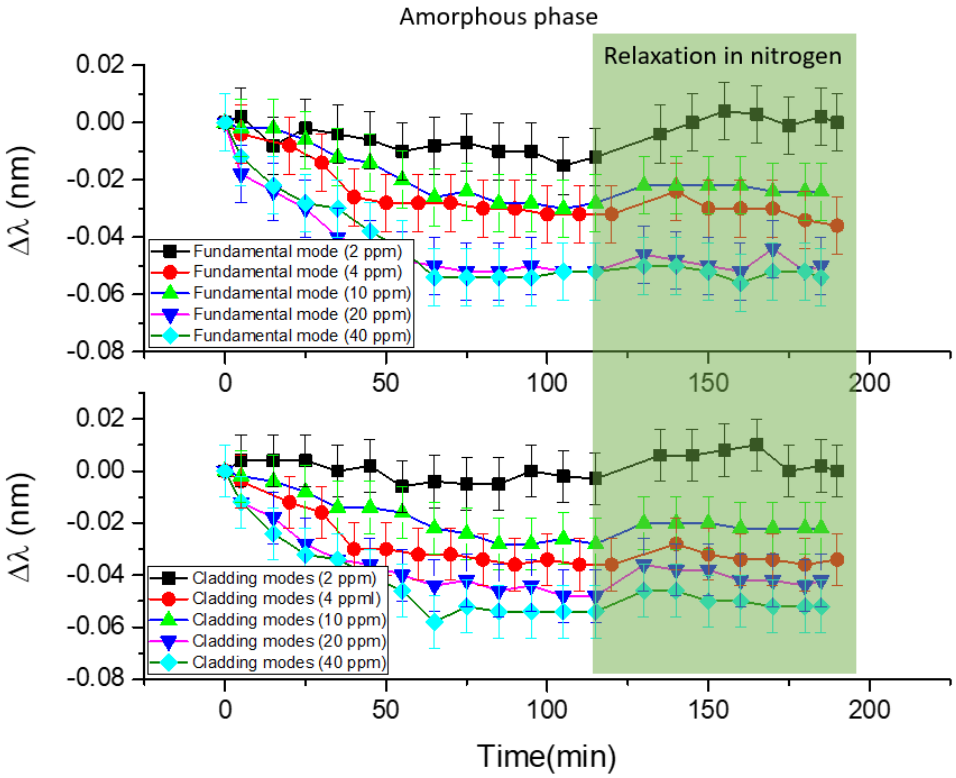

FIGURE 4.1: Spectral shifts vs time of the fundamental and cladding modes of a TOFBG grating overlaid with an amorphous P(VDF–TrFE–CTFE) polymer thin film. The sensor was exposed to TFE vapors of different concentrations for 2 hours and was let to relax in a nitrogen atmosphere for 1 hour .

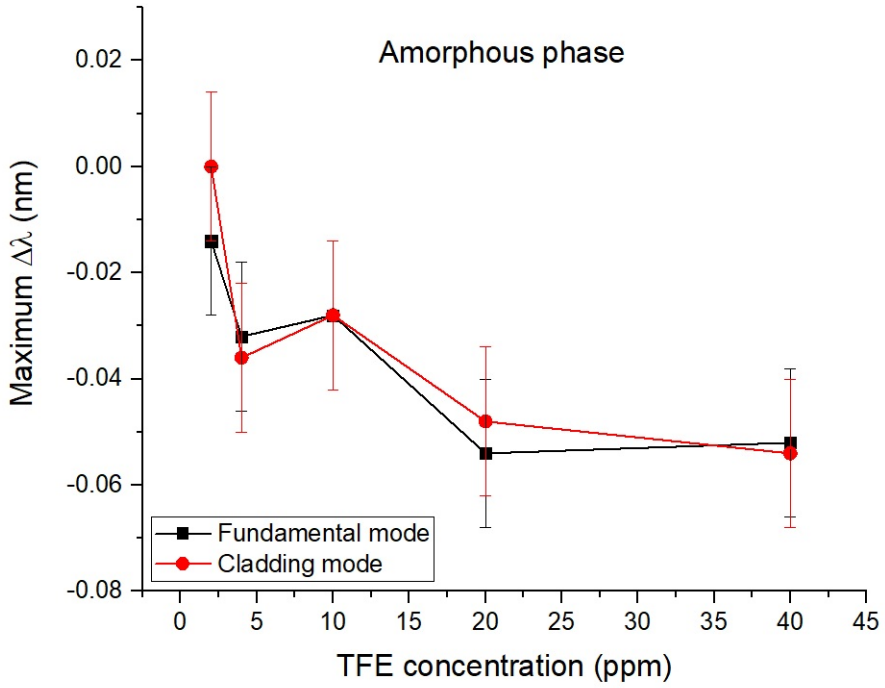

FIGURE 4.2: The maximum shift of the fundamental and the cladding modes, observed for each concentration of TFE (i.e. the shift after 2 hours of exposure) vs the TFE concentration used for the amorphous P(VDF–TrFE–CTFE) polymer layer.

For the cladding mode, which is modally bound in both the fiber cladding and the overlaid film of the optical fiber, a shift towards blue indicates refractive index changes attributed to both physisorption/chemisorption and strain related effects occurring in the P(VDF–TrFE–CTFE) thin transduction film. A point of particular interest is the magnitude of spectral shift obtained for both the core and cladding modes; this appears to be quite similar for both mode types. This fact further strengthens the assumption that the negative spectral shifts observed for the core and cladding modes, are predominately related to strain effects taking place in the P(VDF–TrFE–CTFE) polymer overlayer.

Looking at Figs.(4.1,4.2) for the sensor overlaid with P(VDF–TrFE–CTFE) in the amorphous phase, it is made clear that there is a relation between the spectral shifts and the concentration of TFE. The more the concentration of TFE, the more our spectra shift towards blue. Typical rise up time for the core and cladding spectral shifts reaching plateau are of the order of 60 min, for sensors overlaid with

P(VDF–TrFE–CTFE) in the amorphous phase. Accordingly, studies were performed for investigating the recovery behaviour of this sensing probe. After the $\Delta\lambda$ Bragg and cladding had reached a plateau, nitrogen gas is injected in the chamber at moderate pressures of 1.2 Bar, creating a gas flow for washing out the TFE vapors. Nitrogen gas injection introduces a rather abrupt red shift in both the core and cladding mode notches, which shift tends to stabilise after characteristic times of 10 min. This indicates that residues of TFE physisorbed onto the P(VDF–TrFE–CTFE) surface may have been removed from the gas flow. However, for prolonged recovery phases (longer than 1h) a slow and spectrally shallow blue shift behaviour returns. This might be an indication that TFE is being absorbed by the polymer in greater depths, while continuing to diffuse inside of it even after the gas has been flushed out.

4.1.2 TFE sensing using policrystalline and thermally poled P(VDF–TrFE–CTFE) overlaid TOFBG

For the crystalline phase, the same things seem to apply as in the amorphous phase [Figs.(4.3,4.4)]. The major difference is that the magnitude of the shifts seem to shrink the larger the concentration of TFE is. It is possible that by increasing the crystallinity of the polymer with annealing we give raise to an elasto-optic effect that was latent in the amorphous phase. The strain induced by the polymer-TFE interaction may cause an increase to the refractive index of the polymer. An increase of the refractive index could explain why the shifts become smaller and smaller as the concentration of the gas increases, if the red shift due to the elasto-optic effect is greater than the blue shift due to the mechanical compression of the grating.

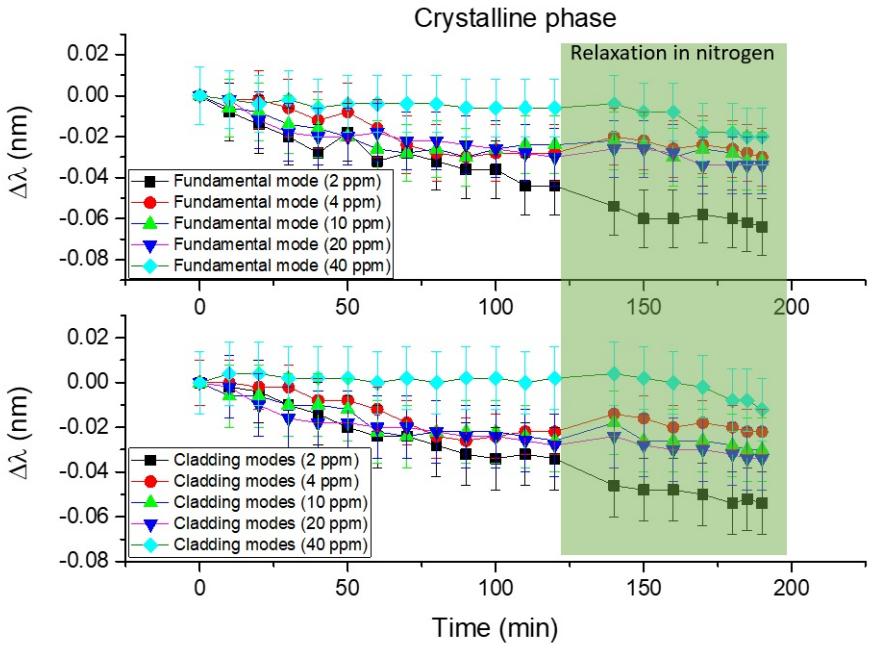

FIGURE 4.3: Spectral shifts vs time of the fundamental and cladding modes of a TOFBG grating overlaid with a crystalline P(VDF–TrFE–CTFE) polymer thin film. The sensor was exposed to TFE vapors of different concentrations for 2 hours and was let to relax in a nitrogen atmosphere for 1 hour .

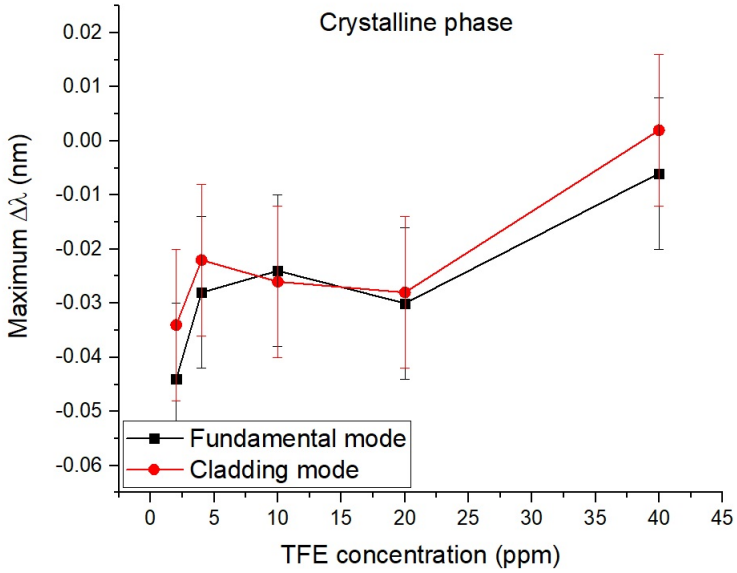

FIGURE 4.4: The maximum shift of the fundamental and the cladding modes, observed for each concentration of TFE (i.e. the shift after 2 hours of exposure) vs the TFE concentration used for the crystalline P(VDF–TrFE–CTFE) polymer layer.

To study the poled phase of the polymer,our sensor was thermally poled at 100 °C under 8 MV/m for 1 hour. The poled sample was the exposed to 2 ppm of TFE. In Fig.(4.5) are presented, the spectral shifts of the fundamental and cladding mode ($\sim$1530.7 nm) for different P(VDF-TrFE-CTFE) polymer film phases, when exposed to 2 ppm of TFE gas. We observe that the curves for the poled and the annealed phase are very similar. Due to the low fields applied we expect that the solely annealed and thermally poled sample will exhibit similar crystallisation characteristics, resulting in similar $\Delta\lambda(t)$ curves.

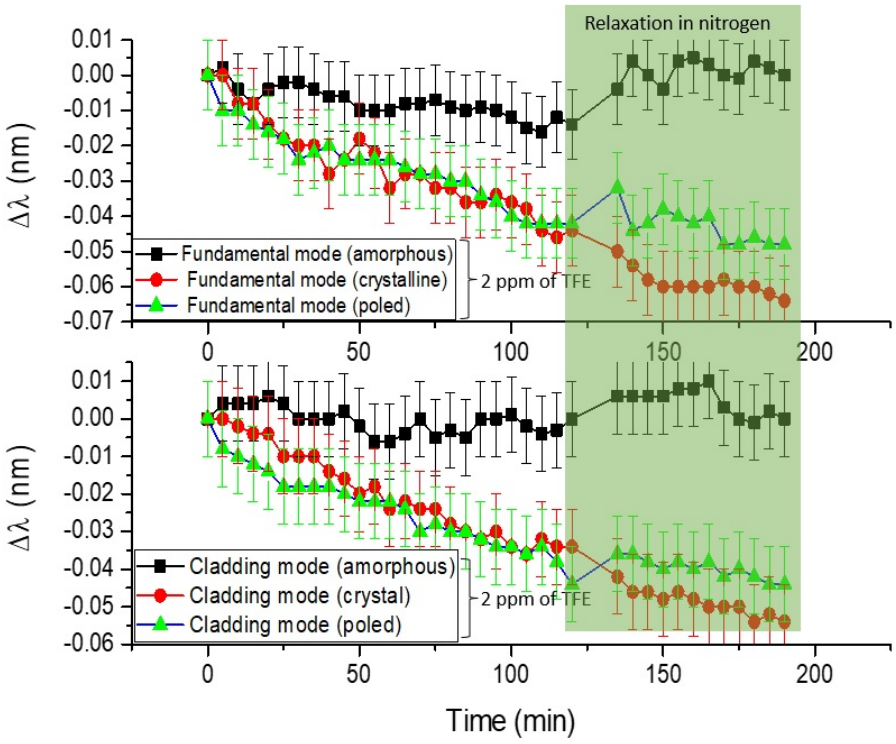

FIGURE 4.5: Spectral shifts vs time of the fundamental and cladding modes of our sensor. Comparison of the different phases of the polymer film.

4.1.3 Study on the reproducibility of results

Finally, to establish the repeatability of results, a new amorphous P(VDF–TrFE–CTFE) overlaid TOFBG probe was fabricated and took repeated measurements for 2 ppm of TFE, while applying intermediate annealing phase between different runs. Results are presented in Fig.(4.6).

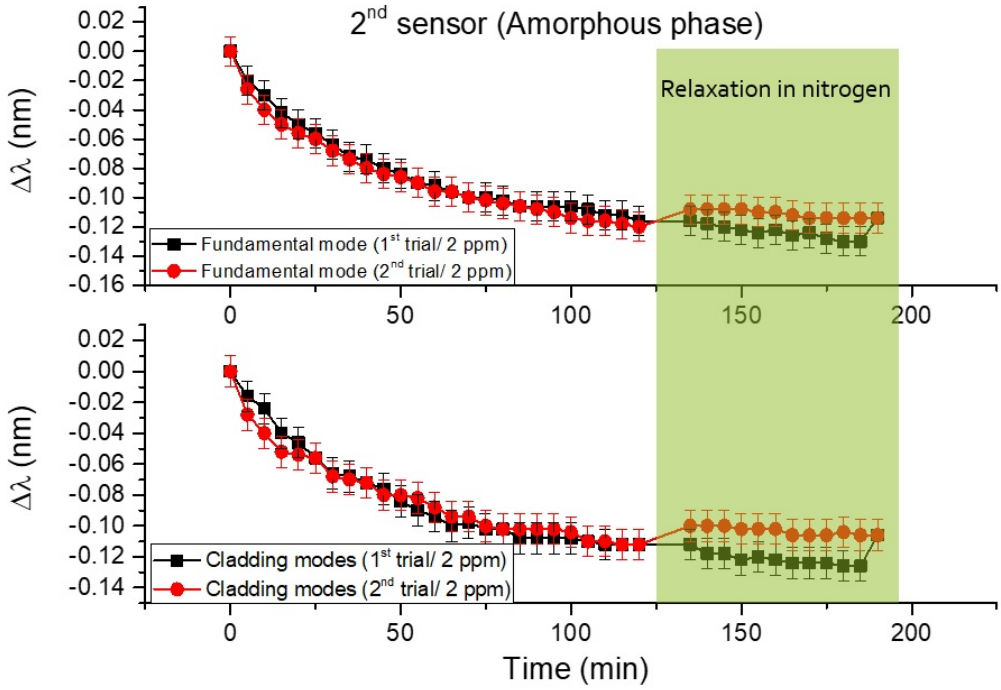

FIGURE 4.6: Spectral shifts vs time of the fundamental and cladding modes of a new sensor. Two measurements for the same concentration of TFE are made.

In Fig.(4.6) it is made obvious that exposure to same concentrations produce similar results. Therefore, by applying consecutive annealing phases, the same sensing probe can be reused, without exhibiting significant hysteresis for the concentration conditions examined.

Another thing to note is the difference between the two sensors shown in subsections 4.1.1-4.1.2 and 4.1.3. It is obvious that sensor of 4.1.3 produces considerably higher shifts than the one presented at 4.1.1-4.1.2. This can be attributed to the difference between the thickness of the polymer film for the two sensors. A thicker film may include more sights from which TFE can be absorbed/interact with the polymer, resulting in more noticeable shifts. However, as it was already discussed, if the film becomes too thick all effects to the fiber may be completely cancelled, as the polymer-environment interface is too far away from the cladding.

4.2 PFOA sensing in aqueous solutions

To study the sensitivity of our sensor to PFOA, we first prepare aqueous solutions of PFOA of different concentrations. Namely, aqueous solutions of 5, 10, 20 and 50 ppm were prepared. The P(VDF–TrFE–CTFE) overlaid TOFBG probe was exposed to those solutions and spectra were collected as a function of time. Similarly to the experiments with TFE, the sensitivity of the sensor was studied as a function of the different phases of the P(VDF–TrFE–CTFE) polymer (amorphous, crystalline and thermally poled). As discussed in Section 3.3.2., the sensor is first submerged in a puddle of deionised (DI) water to collect data regarding the effect of the solvent and condition the sensor, before it is exposed to the PFOA solution. After that, the sensor was submerged in DI water once more to be cleaned of any PFOA residue. The sensor is submerged in DI water for a total of 40 minutes before it is immersed again in the PFOA solution for another 40 minutes. Spectra are collected every 5 minutes for both processes. Again, the spectral shifts are shown as a function of time.

Results are presented in Figs. (4.7, 4.8, 4.9).

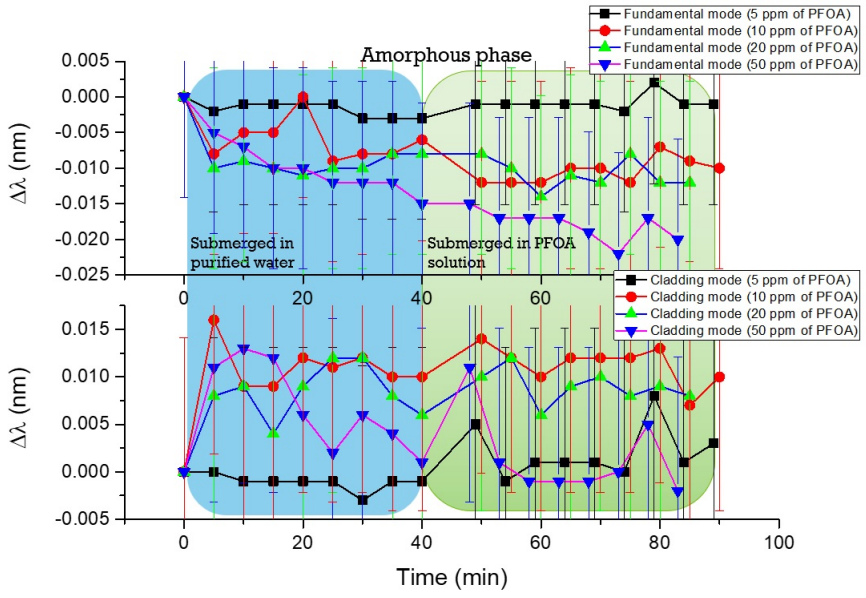

FIGURE 4.7: Spectral shifts vs time of the fundamental and cladding modes of our sensor. The P(VDF–TrFE–CTFE) overlaid TOFBG probe was studied for film being in its amorphous phase.

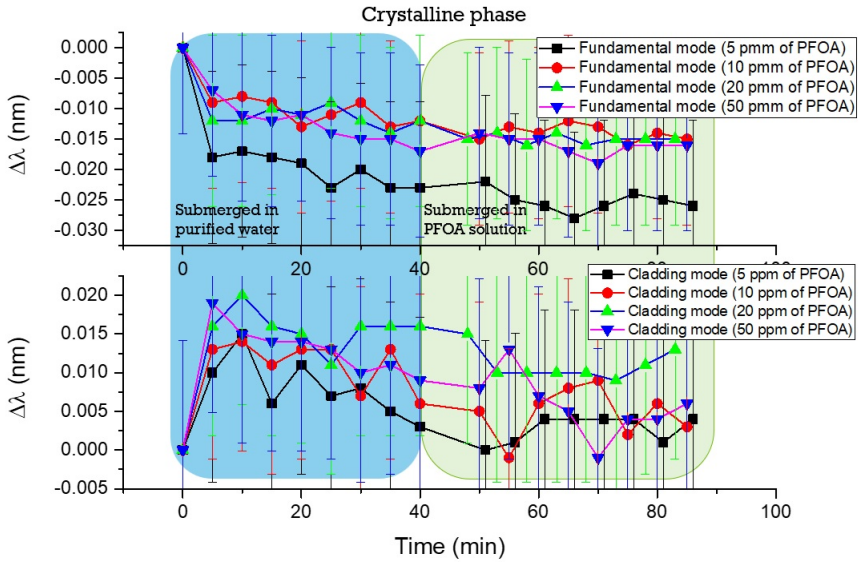

FIGURE 4.8: Spectral shifts vs time of the fundamental and cladding modes of our sensor. The P(VDF–TrFE–CTFE) overlaid TOFBG probe was studied for film being in its crystalline phase.

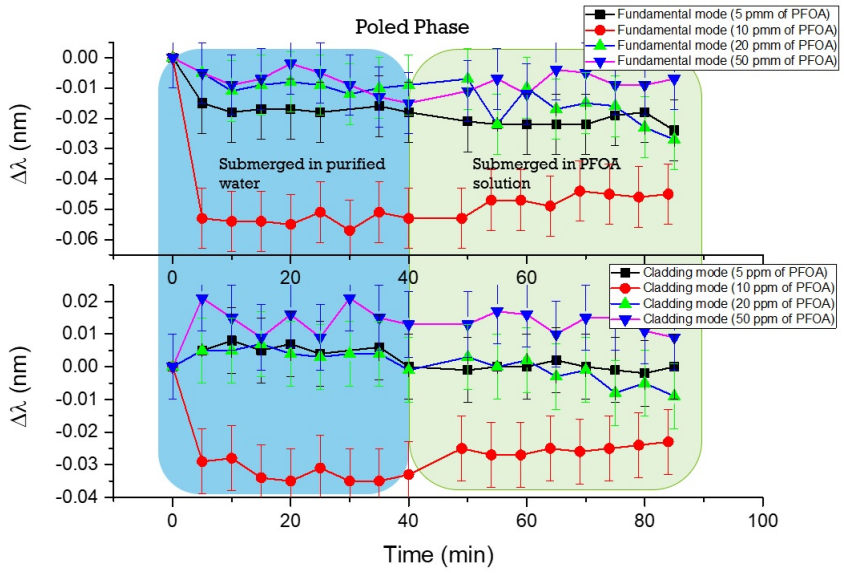

FIGURE 4.9: Spectral shifts vs time of the fundamental and cladding modes of our sensor. The P(VDF–TrFE–CTFE) overlaid TOFBG probe was studied for film being in its poled phase.

In Fig(4.7) the spectral shifts vs time for the fundamental and the cladding mode ($\sim$ 1530.7 nm) for different aqueous solutions of PFOA, are presented. The amorphous phase of the polymer was studied first. All the graphs have been split in two

different areas; one that depicts the spectral shifts while the P(VDF–TrFE–CTFE) overlaid TOFBG probe is submerged in DI water and one that depicts the spectral shifts while the probe is submerged in the PFOA solution. When the P(VDF–TrFE–CTFE) overlaid TOFBG probe is first submerged in DI water a slight shift towards blue is observed for the fundamental mode. This is most likely caused by the induced strain in the polymer due to hydrophobic interactions. Molecules of hydrophobic substances (like P(VDF–TrFE–CTFE)), when surrounded by water, tend to agglomerate in order to reduce their surface area that is exposed to water. It is possible that, by agglomerating, the molecules of the polymer squeeze the fiber grating causing this shift. On the other hand, it is observed that the cladding mode near 1530.7 nm slightly drifts to larger wavelengths. This could be happening for two reasons; either the mechanical strain due to the polymer-water hydrophobic interaction triggers a weak elasto-optic effect (similarly to what was hypothesized in the case of TFE), inducing a refractive index raise in the cladding area, or, by submerging P(VDF–TrFE–CTFE) overlaid TOFBG probe in DI water, a higher refractive index liquid, the effective refractive index in the cladding-environment interface is slightly raised, causing a small shift to red. Either way, the shifts that are observed are quite small. They could very much be just measurement errors. Unfortunately, the small shifts persist even when we submerge our sensor in the PFOA solutions. To be precise, there is little to no change when the DI water is switched with the PFOA solution, meaning that our sensor does not seem to interact with the measurand in any way.

Unfortunately, this picture seems to persist for all polymer phases and all PFOA concentrations; no significant changes seen to occur with the addition of PFOA. This is indicative that no significant interactions happen between the polymer and the measurand. The agglomeration of the polymer molecules due to the hydrophobic interactions may be to blame for that. As the polymer molecules aggregate, making it denser, it is quite possible that surface defects through which PFOA could be absorbed or interact with the polymer (such as pores), are becoming less or get eliminated all together.

4.3 SEM data

Finally, SEM images of P(VDF–TrFE–CTFE) overlaid fibers are presented. Namely, three samples were studied: 1) a fiber that has been overlaid with P(VDF–TrFE–CTFE) and annealed to 70 °C 2) a fiber that has been overlaid with P(VDF–TrFE–CTFE), annealed at 70 °C and exposed to 2 ppm of TFE and 3) a fiber that has been overlaid with P(VDF–TrFE–CTFE), annealed to 70 °C, exposed to 2 ppm of TFE and annealed at 130 °C for 15 minutes for reconditioning the transductor.

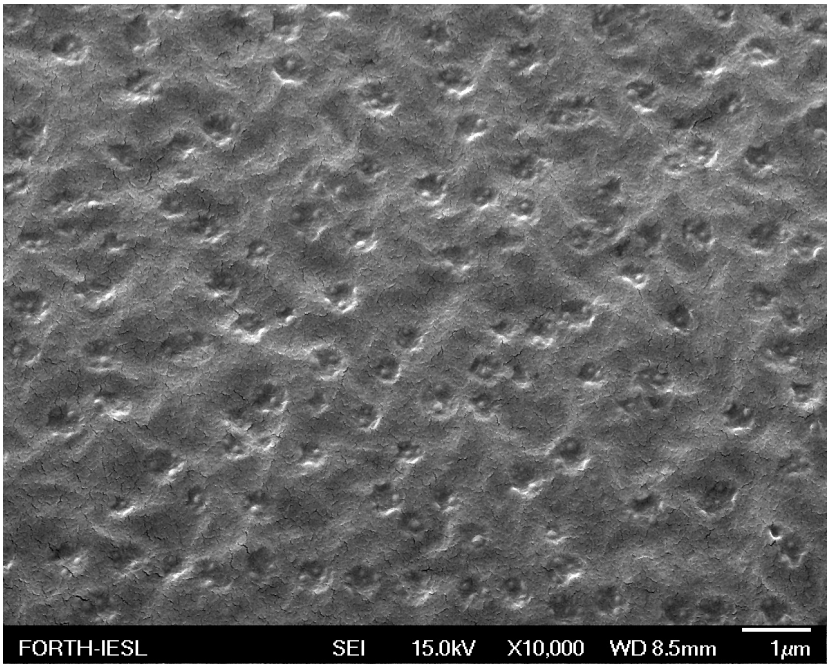

FIGURE 4.10: SEM image of the surface of the amorphous P(VDF–TrFE–CTFE) polymer film of a pristine sample.

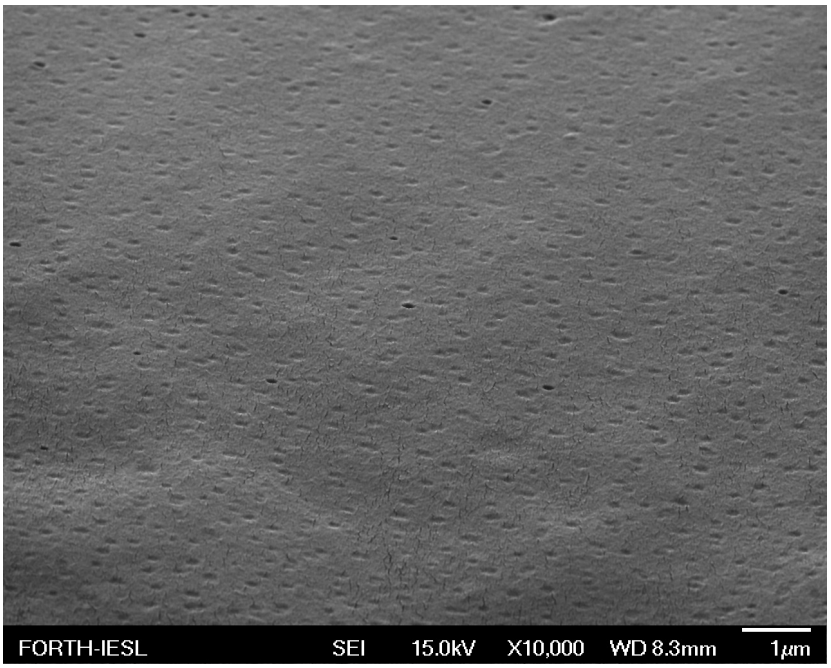

FIGURE 4.11: SEM image of the surface of the amorphous P(VDF–TrFE–CTFE) polymer film exposed to 2 ppm of TFE.

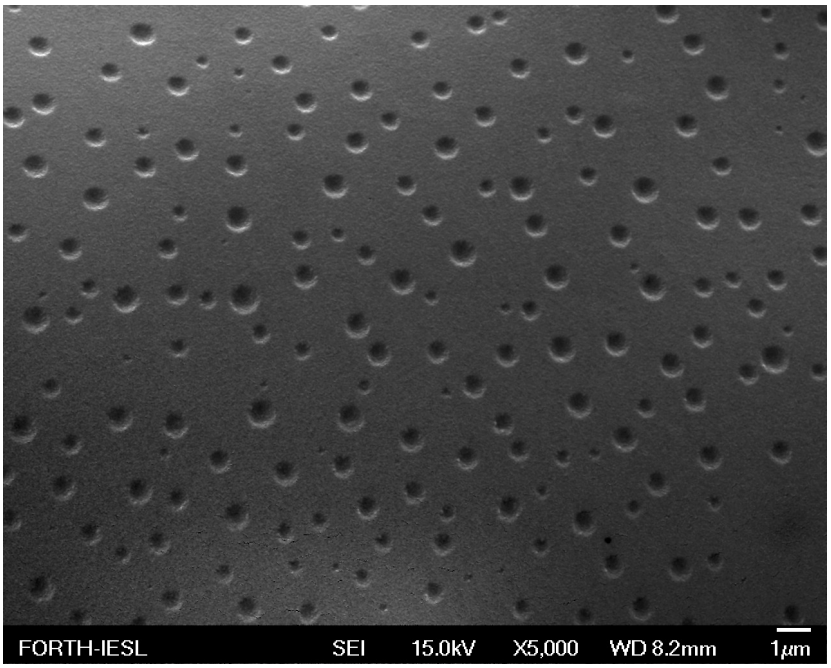

FIGURE 4.12: SEM image of the surface of amorphous P(VDF–TrFE–CTFE) polymer film of a sample exposed to 2 ppm of TFE and annealed to 130 °C for 15 minutes.

The results of Fig(4.10) show that the film annealed at 70°C possibly exhibits some crystallinity, appearing as dot-shape domains of typical dimensions of >0.5 μm. Accordingly, by exposing the film to TFE [Fig(4.11)] these crystalline domains vanish, indicating a possible surface dissolution process by the TFE. Finally, the re-conditioned film at 130 °C [Fig(4.12)] shows again a large scale porosity, however without the nano-crystalline domain of Fig(4.10), indicating only a partial reversibility to the initial condition. These SEM results indicate that a possible transduction mechanism between the P(VDF–TrFE–CTFE) polymer and TFE is related to surface dissolution effects, which in turn can also introduce swelling and volume dilation effects of the polymer films, observed in the TOFBG spectral measurements.

Chapter 5

Conclusion

In this master thesis we presented the development and capabilities of an optical fiber chemo-sensor, sensitive to perfluorinated substances. Our sensor was based on the sensing capabilities of a TOFBG in overlaid with a P(VDF–TrFE–CTFE) polymer film, that was used as a transducer. The P(VDF–TrFE–CTFE) overlaid TOFBG probe was exposed to TFE gas and PFOA aqueous solutions. The spectral shifts of the fundamental mode (1550.5 nm) and the cladding modes (1530.7 nm), due to the P(VDF–TrFE–CTFE) polymer film-measurand interaction, were recorded as a function of time. Our sensor's sensitivity to different concentrations of TFE gas and PFOA aqueous solutions, was tested; being able to sense concentrations as low as 2 ppm. We also tested our sensor's response and sensitivity in relation with the different structural phases of the P(VDF–TrFE–CTFE) polymer film (amorphous, crystalline and thermally poled).

The results we gathered using TFE gas proved to be quite promising, with the collected SEM data indicating a direct link between amorphization of the polymer surface and exposure to the perfluorinated vapors. On one of our sensors' we recorded spectral shifts ranging between -0.006 and -0.054 ($\pm$0.014) nm, depending on the concentration of TFE and the phase of the polymer. While the magnitude of the shifts remains the same for the different phases of the polymer, the relation between shift magnitude and concentration differs depending on the phase. For the amorphous phase, the magnitude of the shifts increases with the concentration, while for the poled and the annealed phase the opposite happens, possibly due to the rise of an elasto-optic effect. We also fabricated a second sample to test our sensors consistency. We collected two sets of data for the same concentration and found that the

data curves are almost identical. This sample produced spectral shifts of the order of magnitude of -0.12 ($\pm$0.014) nm. This indicates that depending on the fabrication process, and especially the polymer film thickness, one sample can produce spectral shifts of larger or smaller magnitude.

On the other hand, our results using PFOA were not as fruitful. Our sensor does not seem to respond to PFOA solutions; possibly due to the hydrophobic water-polymer interaction. Namely, we observe a slight spectral shift when the sample is submerged in water, between 0 and -0.05 ($\pm$0.014) nm for the fundamental mode. However, when the sample is submerged in the PFOA solution no major changes seem to occur. Again, we studied the amorphous, crystalline and poled phases for concentrations between 5 and 50 ppm, but our results do not lead us to any credible conclusions.

Regarding the sensor's fabrication process, a way to reliably control the thickness and homogeneity of the polymer film, proves to be crucial for real life applications, as it greatly affects the sensor's sensitivity. Finally, apart from the P(VDF–TrFE–CTFE), other polymers of the PVDF family should be tested as transducers.

References

1. Sirkis, J. *et al.* In-line fiber etalon (ILFE) fiber-optic strain sensors. *Journal of Lightwave Technology* **13,** 1256–1263 (1995).

2. A.H. Hartog A.P. Leach, M. G. Distributed temperature sensing in solid-core fibres. *Electronics Letters* **21,** 1061–1062(1). ISSN: 0013-5194. https://digital-library.theiet.org/content/journals/10.1049/el_19850752 (23 1985).

3. Childs, P., Candiani, A. & Pissadakis, S. Optical Fiber Cladding Ring Magnetic Field Sensor. *Photonics Technology Letters, IEEE* **23,** 929 –931 (Aug. 2011).

4. Goldstein, S. R., Peterson, J. I. & Fitzgerald, R. V. A Miniature Fiber Optic pH Sensor for Physiological Use. *Journal of Biomechanical Engineering* **102,** 141–146. ISSN: 0148-0731. eprint: https://asmedigitalcollection.asme.org/biomechanical/article-pdf/102/2/141/5491749/141_1.pdf. https://doi.org/10.1115/1.3138210 (May 1980).

5. Qian, Y., Zhao, Y., lu Wu, Q. & Yang, Y. Review of salinity measurement technology based on optical fiber sensor. *Sensors and Actuators B: Chemical* **260,** 86–105. ISSN: 0925-4005. https://www.sciencedirect.com/science/article/pii/S0925400517324036 (2018).

6. Konstantaki, M., Pissadakis, S., Pispas, S., Madamopoulos, N. & Vainos, N. A. Optical fiber long-period grating humidity sensor with poly(ethylene oxide)/cobalt chloride coating. *Appl. Opt.* **45,** 4567–4571. http://opg.optica.org/ao/abstract.cfm?URI=ao-45-19-4567 (2006).

7. Konstantaki, M. *et al.* Silk Fibroin Enabled Optical Fiber Methanol Vapor Sensor. *IEEE Photonics Technology Letters* **32,** 514–517 (2020).

8. Nedoma, J. *et al.* Analysis of the use of fiber-optic sensors in the road traffic. *IFAC-PapersOnLine* **51.** 15th IFAC Conference on Programmable Devices

and Embedded Systems PDeS 2018, 420–425. ISSN: 2405-8963. https://www.sciencedirect.com/science/article/pii/S2405896318308619 (2018).

9. Crickmore, R., Nash, P., Ab, J. & Centre, W. Fiber optic security systems for land- and sea-based applications (Nov. 2004).

10. Dandridge, A. & Cogdell, G. Fiber Optic Sensors for Navy Applications. *LCS, IEEE* **2,** 81 –89 (Mar. 1991).

11. Woulfe, P., Sullivan, F. & O'Keeffe, S. Optical fibre sensors: their role in in vivo dosimetry for prostate cancer radiotherapy. *Cancer Nanotechnology* **7** (Oct. 2016).

12. Liokumovich, L., Medvedev, A., Kotov, O., Markov, S. & Nikolaev, V. Fiber optic sensors for environmental monitoring. *Linnaeus Eco-Tech,* 527–530 (Mar. 2019).

13. Mignani, A. G., Brenci, M. & Mencaglia, A. Fiber Optic Sensors for Environmental Monitoring (ed Soares, O. D. D.) 691–708. https://doi.org/10.1007/978-94-011-0035-9_34 (1995).

14. Marie Pospíšilová, G. K. & Trögl, J. Fiber-Optic Chemical Sensors and Fiber-Optic Bio-Sensors. *Sensors* **15,** 25208–25259. doi:10.3390/s151025208 (Sept. 2015).

15. Dong Wang, X. & Wolfbeis, O. S. Fiber-Optic Chemical Sensors and Biosensors (2015-2019). *Analytical Chemistry* **92,** 397–430 (2019).

16. Pissadakis, S. Class-notes on "Advanced Subjects on Photonics (2020).

17. Rüdiger, P. Fiber Bragg Gratings. *RP Photonics encyclopedia.* https://www.rp-photonics.com/fiber_bragg_gratings.html.

18. Xiaoyi Dong Hao Zhang, B. L. & Miao, Y. Tilted Fiber Bragg Gratings: Principle and Sensing Applications. *Photonic Sensors* **92,** 6–30 (2011).

19. Jacques Albert1, L.-Y. S. & Caucheteur, C. Tilted fiber Bragg grating sensors. *Laser Photonics Reviews* **92,** 1–3. doi:10.1002/lpor.201100039 (2012).

20. Et al., T. A. V. How to Test Water for Fluoride. *wikiHow.* https://www.wikihow.com/Test-Water-for-Fluoride#Using-Testing-Strips (2021).

21. Facts About Sarin. *Centers for Disease Control and Prevention.* https://emergency.cdc.gov/agent/sarin/basics/facts.asp (May Page last reviewed: April 4, 2018).

22. BBC. Aum Shinrikyo: The Japanese cult behind the Tokyo Sarin attack. *Centers for Disease Control and Prevention.* https://www.bbc.com/news/world-asia-35975069 (July 2018).

23. Fairuza Faiza Gregory Baxterb, S. C. F. S. M. C. Polyvinylidene fluoride coated optical fibre for detecting perfluorinated chemicals. *Sensors and Actuators B: Chemical* **312,** 1–2. https://doi.org/10.1016/j.snb.2020.128006 (2020).

24. 2,2,2-Trifluoroethanol, 99+%, Thermo Scientific. *Fischer Scientific.* https://www.fishersci.com/shop/products/2-2-2-trifluoroethanol-99-thermo-scientific/AAA1078818.

25. FORANE- isoflurane inhalant. *DailyMed.* https://dailymed.nlm.nih.gov/dailymed/drugInfo.cfm?setid=3d30eb8d-a62e-475f-926b-78ba63bee9c8 (Last Updated October 25, 2021).

26. Unit, H. R. A. PFOA Information Sheet April 2022. *Minnesota Department of Health.* https://www.health.state.mn.us/communities/environment/risk/docs/guidance/gw/pfoainfo.pdf (2022).

27. Lee, B. Review of the present status of optical fiber sensors. *Optical fiber Technology* **9,** 57–79. DOI:10.1016/S1068-5200(02)00527-8 (Apr. 2003).

28. "OFS-A Furukawa company". https://www.ofsoptics.com/optical-fiber-coatings/.

29. B., E. Cable Engineering for Local Area Networks, 161–185 (200).

30. Rüdiger, P. Fibers. *RP Photonics encyclopedia.* https://www.rp-photonics.com/fibers.html.

31. Rüdiger, P. Acceptance angle in fiber optics. *RP Photonics encyclopedia.* https://www.rp-photonics.com/acceptance_angle_in_fiber_optics.html.

32. Pearseal, T. P. Photonics essentials-An introduction with experiments. *Mc Graw-Hill,* 57–79. DOI:10.1016/S1068-5200(02)00527-8 (2002).

33. Winklberger", M. *"Damage detection in thin-walled structures with strain measurements along zero-strain trajectories"* ("Johannes Kepler Universität Linz", "2016").

34. Snyder, A. & Love, J. *Optical Waveguide Theory* https://books.google.gr/books?id=B2CkoAEACAAJ (Kluwer academic publisher, 2000).

35. Gloge, D. Weakly Guiding Fibers. *Appl. Opt.* **10,** 2252–2258. http://opg.optica.org/ao/abstract.cfm?URI=ao-10-10-2252 (1971).

36. Venghaus, H. Wavelength Filters in Fibre Optics. *Springer Series in Optical Science* **123,** 189–192 (2006).

37. Venghaus, H. Wavelength Filters in Fibre Optics. *Springer Series in Optical Science* **123,** 192–195 (2006).

38. Guo, T., González-Vila, Loyez, M. & Caucheteur, C. Plasmonic Optical Fiber-Grating Immunosensing: A Review. *Sensors* **17.** ISSN: 1424-8220. https://www.mdpi.com/1424-8220/17/12/2732 (2017).

39. Albert, J., Shao, L. Y. & Caucheteur, C. Tilted fiber Bragg grating sensors. *Laser and Photonics Reviews* **7,** 83–108. ISSN: 18638880. 10.1002/lpor.201100039 (1 Jan. 2013).

40. Osgood, R. & Meng, X. *Principles of Photonic Integrated Circuits: Materials, Device Physics, Guided Wave Design* ISBN: 9783030651930. https://books.google.gr/books?id=x6QvEAAAQBAJ (Springer International Publishing, 2021).

41. D. K. W. Lam, K. G. Characterization of single-mode optical fiber filters. *Applied Optics* **20,** 440–445 (3 Jan. 1981).

42. Corning®. Corning® SMF-28™ Optical Fiber Product Information. https://www.health.state.mn.us/communities/environment/risk/docs/guidance/gw/pfoainfo.pdf (Apr. 2001).

43. Deroh, M. *et al.* Towards athermal Brillouin strain sensing based on heavily germania-doped core optical fibers. *APL Photonics* **4,** 030801. eprint: https://doi.org/10.1063/1.5085640. https://doi.org/10.1063/1.5085640 (2019).

44. Venghaus, H. Wavelength Filters in Fibre Optics. *Springer Series in Optical Science* **123,** 220–222 (2006).

45. Polyvinylidene Fluoride (PVDF): Properties, Production, Applications. *Matmatch.* https://matmatch.com/learn/material/polyvinylidene-fluoride-pvdf (Accesed, 17 July 2022).

46. Ruan, L. *et al.* Properties and Applications of the β Phase Poly(vinylidene fluoride). *Polymers* **10.** ISSN: 2073-4360. https://www.mdpi.com/2073-4360/10/3/228 (2018).

47. Hu, X., You, M., Yi, N., Zhang, X. & Xiang, Y. Enhanced Piezoelectric Coefficient of PVDF-TrFE Films via In Situ Polarization. *Frontiers in Energy Research* **9** (Aug. 2021).

48. Xu, H. *et al.* Ferroelectric and electromechanical properties of poly(vinylidene-fluoride–trifluoroethylene–chlorotrifluoroethylene) terpolymer. *Applied Physics Letters* **78,** 2360–2362. https://doi.org/10.1063/1.1358847 (2001).

49. Santucci, S. & Esposito, V. in *Encyclopedia of Materials: Technical Ceramics and Glasses* (ed Pomeroy, M.) 369–374 (Elsevier, Oxford, 2021). ISBN: 978-0-12-822233-1. https://www.sciencedirect.com/science/article/pii/B9780128035818120715.

50. Opaprakasit, P., Petchsuk, A., Painter, P. & Malkov, S. Dynamic 2D-FTIR Spectroscopic Studies Poly(Vinylidine Fluoride) (July 2022).

51. Bauer, F. Relaxor fluorinated polymers: novel applications and recent developments. *IEEE Transactions on Dielectrics and Electrical Insulation* **17,** 1106–1112 (2010).

52. John Wiley Sons, I. 2,2,2-Trifluoroethanol. *SpectraBase.* https://spectrabase.com/spectrum/Hla4RVM1xQH (Accesed, 15 July 2021).

53. 2,2,2-Trifluoroethanol: Safety Data Sheet 2101303. *Synquest Laboratories Inc.* **77.** http://synquestlabs.com/msds/2100/2101-3-03.pdf (58 Jan. 2016).

54. Siegemund, G. *et al.* Fluorine Compounds, Organic. https://onlinelibrary.wiley.com/doi/abs/10.1002/14356007.a11_349 (2000).

55. De Voogt, P. in *Encyclopedia of Toxicology (Third Edition)* (ed Wexler, P.) Third Edition, 802–805 (Academic Press, Oxford, 2014). ISBN: 978-0-12-386455-0. https://www.sciencedirect.com/science/article/pii/B9780123864543005273.

56. Database, G. S. Record of Perfluorooctanoic Acid. *Institute for Occupational Safety and Health of the German Social Accident Insurance (IFA).* https://gestis.dguv.de/data?name=493012&lang=en (Accesed, 15 July 2021).

57. Perfluorooctanoic Acid. *ChemBK*. https://www.chembk.com/en/chem/Perfluorooctanoic\%20acid (Accesed, 15 July 2022).